View metadata, citation and similar papers at core.ac.uk

brought to you by CORE

provided by NASA Technical Reports Server

CONFIDENTIAL

Copy 5
RM E53H28

NACA RM E53H28

NACA

RESEARCH MEMORANDUM

PERFORMANCE CHARACTERISTICS OF A DOUBLE-CYLINDRICAL-SHROUD EJECTOR NOZZLE

By Eli Reshotko

Lewis Flight Propulsion Laboratory
Cleveland, Ohio

CLASSIFICATION CHANGED

To UNCLASSIFIED

By authority of NACA Res abs TRN-119 Date effective Aug. 16, 1957
AMT 10-16-57

LIBRARY COPY

NOV 27 1953

LANGLEY AERONAUTICAL LABORATORY
LIBRARY, NACA
LANGLEY FIELD, VIRGINIA

CLASSIFIED DOCUMENT

This material contains information affecting the National Defense of the United States within the meaning of the espionage laws, Title 18, U.S.C., Secs. 793 and 794, the transmission or revelation of which in any manner to an unauthorized person is prohibited by law.

NATIONAL ADVISORY COMMITTEE
FOR AERONAUTICS

WASHINGTON

November 24, 1953

CONFIDENTIAL

NASA Technical Library
3 1176 01435 2836

NACA RM E53H28

NATIONAL ADVISORY COMMITTEE FOR AERONAUTICS

RESEARCH MEMORANDUM

PERFORMANCE CHARACTERISTICS OF A DOUBLE-CYLINDRICAL-SHROUD EJECTOR NOZZLE

By Eli Reshotko

3006

CF-1

SUMMARY

The performance characteristics of a double-shroud ejector were investigated for the purpose of evaluating its effectiveness as an exit nozzle. Calculations based on ejector performance data, taken with the ejector discharging into quiescent air, indicate that thrust performance on the order of ideal nozzle thrust may be obtained over a Mach number range of 0.8 to 2.3 from a double-shroud ejector. Maximum thrust is obtained with maximum pressure recovery of the secondary- and tertiary-air inlets. Short secondary shrouds, high secondary weight flows, and low (not necessarily zero) tertiary weight flows are desirable.

The results of a simplified theoretical analysis are in fair agreement with those experimentally obtained.

INTRODUCTION

Numerous investigations have recently been made of the performance characteristics of ejectors. The ejector appears attractive for tailpipe and other cooling, since it can perform its cooling function and still give greater thrust than an uncooled convergent nozzle over a wide range of Mach number. In a single-shroud ejector, the secondary flow may be used for afterburner cooling; in the double-shroud ejector, the secondary flow may be used for afterburner cooling and the tertiary flow for structural cooling.

The pumping characteristics and gross thrust performance of single-shroud ejectors with both cylindrical and conical shrouds are given in references 1 to 4. References 5 and 6 are concerned with double-shroud ejector performance, but principally for the special case of secondary total pressure equal to tertiary total pressure.

CONFIDENTIAL

In considering the ejector as an exhaust nozzle, it is reasoned that the secondary flow cushions the expansion of the primary stream in such a way that the primary flow approximates an isentropic expansion. If the ejector is to be considered as a variable nozzle, then it must operate close to design conditions and without overexpansion over a wide range of pressure ratio. Isentropic expansion can be more closely approximated by a double-shroud ejector than by a single-shroud ejector of the same over-all diameter ratio, provided that the secondary and tertiary flows enter the ejector at their proper respective pressure levels, which are generally not the same.

3006

The purpose of this investigation was, therefore, to determine the effect of varying shroud lengths and weight flows on the performance characteristics of a double-cylindrical-shroud ejector. The investigation was restricted to a single pair of shroud diameters; the ejector, in the experimental portion of the investigation, discharged into quiescent air. An extension to the ejector theory of reference 1 is presented in order to predict the performance of a double-shroud ejector. Comparison is made with the experimentally obtained performance in order to show the capabilities and limitations of the theory. This investigation was conducted at the NACA Lewis laboratory.

APPARATUS AND PROCEDURE

A sectional drawing of the ejector used in this investigation is shown in figure 1. The tertiary-shroud diameter was chosen as that giving the area ratio corresponding to a pressure ratio of 10 for isentropic expansion of the primary flow. The secondary-shroud diameter was chosen as that giving the largest Mach number at the tertiary exit with the assumption of no secondary or tertiary flow. The secondary- and tertiary-shroud diameter ratios are 1.171 and 1.396, respectively. The method used in these calculations is based on the development in appendix B, part I. The secondary and tertiary flows each entered the ejector through a separate set of eight equally spaced tubes, as indicated in figure 1. Preliminary total-pressure surveys were taken around the secondary and tertiary annuli with zero primary flow. The permanent secondary and tertiary total-pressure tubes were placed at angular locations, which gave average readings in the preliminary surveys. Secondary-shroud length was varied from 0.11 to 0.51 primary-nozzle diameter by translation of the primary nozzle with a fixed secondary shroud. Tertiary-shroud length could be varied about 0.35 primary-nozzle diameter by translation of the secondary shroud. Two additional tertiary-shroud pieces were provided to allow variation of the tertiary-shroud-length increment L_t' over a range including 0.16 to 0.86 primary-nozzle diameter.

[redacted]

3006

The ejector was mounted in a duct station as shown in figure 2. Heated dry air was available through the top header. The operating total temperature varied between 180° and 220° F, and the dewpoint between 0° and -15° F. The combination of dewpoint and total temperature was at all times checked to satisfy the criteria for condensationless flow of reference 7. Varying nozzle pressure ratios were provided by controlling the pressure in the exhauster line. The inlet total pressure was relatively constant at approximately atmospheric pressure. For each setting of exhaust-line pressure and secondary and tertiary weight flows, readings were taken of the secondary and tertiary total pressures. These pressures were read on a mercury manometer board to 0.05 inch. It is estimated that these pressures are correct to ±3 percent. The wall pressure taps indicated in figure 1 were recorded for only a few runs. Both secondary and tertiary weight flows were originally measured with rotameters; however, an orifice meter was later required for the higher secondary weight flows. The arrangement of these flow meters is indicated in figure 2.

CF-1 back

The combinations of secondary- and tertiary-shroud lengths tested in this investigation are listed in table I. For each shroud length with secondary-shroud-length ratio $L_s/D_p \geq 0.21$, data were obtained for the 16 weight-flow combinations that arise from varying both secondary and tertiary weight-flow parameters $\frac{W_s}{W_p}\sqrt{\frac{T_s}{T_p}}$ and $\frac{W_t}{W_p}\sqrt{\frac{T_t}{T_p}}$, (hereafter symbolized as $(\omega\sqrt{\tau})_s$ and $(\omega\sqrt{\tau})_t$, respectively) through the values 0, 0.015, 0.030, and 0.045. For the shroud-length combinations with $L_s/D_p = 0.11$, only the data for $(\omega\sqrt{\tau})_s = 0$ could be obtained, as the short secondary shroud caused complete blockage of the secondary-flow feeder tubes. For the combinations $L_s/D_p = 0.21$, $L_t/D_p = 0.54$, and $L_s/D_p = 0.21$, $L_t/D_p = 0.90$, additional data were taken for $(\omega\sqrt{\tau})_s = 0.06$, 0.09, 0.11, and the aforementioned values for the tertiary flow; for the combination $L_s/D_p = 0.41$, $L_t/D_p = 0.74$, additional data were taken for $(\omega\sqrt{\tau})_s = 0.06$, 0.09, 0.12, and the aforementioned values for the tertiary flow.

All symbols are defined in appendix A.

RESULTS AND DISCUSSION

The ejector performance data obtained in this investigation are presented in figure 3, which includes data over the complete range of tertiary-shroud-length increment for a single secondary-shroud length and over the complete range of secondary-shroud length for a single

[redacted]

tertiary-shroud-length increment. Also presented are the data for the combination of the shortest secondary-shroud length and shortest tertiary-shroud-length increment (fig. 3(a)). The nozzle pressure ratio indicated (less than unity) is the reciprocal of the conventional nozzle pressure ratio.

Examination of the curves indicates that for moderate or long shrouds at low nozzle pressure ratios, the minimum secondary and tertiary pressure ratios are constant independent of primary pressure ratio. At a certain pressure ratio, the flow breaks away from the shroud (fig. 3(c), e.g.); and, at higher nozzle pressure ratios, the secondary pressure ratio becomes directly dependent on the primary. The secondary performance is similar to the single-shroud ejector performance of reference 1. The tertiary pressure ratio for high nozzle pressure ratios is approximately equal to the nozzle pressure ratio. It is to be noted from examination of figures 3(c), (d), (h), (i), and (j) that the secondary pressure ratios are almost completely independent of tertiary weight flow and shroud length. This fact is discussed further when the assumptions made in the double-shroud ejector theory of appendix B are considered.

3006

The variation of minimum secondary pressure ratio with tertiary-shroud-length increment is plotted in figure 4. Except at short secondary shroud lengths and high secondary weight flows, the minimum secondary pressure ratio is relatively independent of the tertiary-shroud-length increment and the tertiary weight flow. For high secondary weight flows there is a slight variation with tertiary-shroud-length increment, while for short secondary-shroud lengths there is some variation with tertiary weight-flow parameter.

Comparison of Experimental Data with Theoretical Analysis

An approximate theory for the prediction of ejector performance is presented in appendix B. The assumptions in this theory are as follows: (1) The shroud lengths are sufficiently short that no mixing takes place between adjacent streams. (2) The primary expansion is isentropic in the cases involving secondary flow. (Where no secondary flow is involved, a free-jet expansion is obtained as the simultaneous solution of the continuity and momentum equations.) (3) The secondary flow and tertiary flow expand to sonic condition at the extremities of their respective shrouds. (4) In the case of tertiary flow, the secondary expands isentropically within the tertiary shroud.

In figure 5, the data of figure 4 are replotted against secondary-shroud-length ratio for comparison with the values predicted by the theory of appendix B, part II. The values obtained experimentally are generally below the theoretical prediction; again, it is seen that

for the short secondary-shroud lengths, there is a slight variation with tertiary weight-flow parameter. For short secondary-shroud lengths and high secondary weight flows, values of minimum secondary pressure ratio are obtained that are significantly above the theoretical prediction. The reason for this is not known. It is also seen in the case of $(\omega\sqrt{\tau})_s = 0$ that the theory indicates a shorter critical secondary-shroud length than was obtained experimentally. This shorter length is perhaps due to the inability of the Prandtl-Meyer expansion to describe adequately a three-dimensional effect.

3006

Figure 6 is presented in order to help evaluate the effect of the secondary expansion on the tertiary expansion. There is fair agreement (± 0.015) between the theoretical prediction and the average experimental value of minimum tertiary pressure ratio for given secondary and tertiary weight flows. It is observed that, for $L_s/D_p > 0.2$, minimum tertiary pressure ratio decreases with increasing secondary-shroud length. This variation is not obtained theoretically. The variation of minimum tertiary pressure ratio with tertiary-shroud length is slight.

Therefore, in the absence of experimental information, application of the presented approximate theory to calculate pressures for given weight flows will give some indication of the obtainable performance. However, the inverse calculation of weight flows for given pressures may be greatly in error.

Ejector Thrust Performance

The thrust characteristics of the double-shroud ejector are calculated on an incremental thrust basis. The incremental thrust ratio is defined as $\frac{F_n - (F_n)_c}{(F_n)_{c,i}}$, where the F_n quantities are net internal thrusts. The comparison indicated by the incremental thrust ratio is for equal throat areas (equal primary weight flow); thus, the incremental thrust ratios are an indication of the thrust augmentation due to the secondary and tertiary shrouds. The expressions for incremental thrust ratio are derived in appendix C. Momentum losses due to friction are entirely neglected. Since net thrusts are involved, some assumption must be made regarding the flight plan for the configuration of which the ejector is a part. These flight plan assumptions are given in appendix D and in figure 7. It was also assumed that the secondary air provided all the afterburner cooling, while the tertiary air was assumed unheated. The temperature rise of the secondary air was estimated from information in reference 8.

Incremental thrust ratio as a function of secondary weight-flow parameter is plotted in figure 8 for the most promising shroud-length combinations at six values of flight Mach number. The most promising shroud-length combination for a given Mach number is that which had the largest secondary and tertiary pressure ratios at the nozzle pressure ratio corresponding to the Mach number. The most promising shroud-length combinations have short secondary shrouds. The incremental thrusts for these shroud-length combinations increase continuously with increasing secondary weight flow. For $M_0 \leq 1.1$, the shroud-length combination $L_s/D_p = 0.21$, $L_t/D_p = 0.54$ with zero tertiary weight flow gives the highest incremental thrust ratios of the secondary weight-flow range. For $M_0 \geq 1.4$, the shroud-length combination $L_s/D_p = 0.21$, $L_t/D_p = 0.90$ with $(\omega\sqrt{\tau})_t = 0.015$ generally gives the largest incremental thrusts. Two limiting lines are indicated in each part of figure 8, the maximum values of the secondary weight flow that can be taken in (1) through an auxiliary free-stream normal-shock inlet and (2) through a boundary-layer scoop, as determined from the experimental data using the maximum available secondary pressure ratios of figure 7. (The maximum secondary weight flow available to the ejector is slightly less than the preceding maximum, since there is a total-pressure loss associated with the addition of heat to the secondary flow in the afterburner. Since no assumptions are made regarding the afterburner dimensions, this reduction in secondary weight flow is not considered.) Therefore, the largest incremental thrust is obtained at the largest available secondary weight flow, and the latter is a function of the auxiliary inlet performance. The optimum value of the tertiary weight-flow parameter was about 0.015 for the free-stream scoop at all Mach numbers. For the boundary-layer scoop, the optimum values of the tertiary weight-flow parameter were zero for M_0 less than about 1.2, 0.030 for M_0 between 1.2 and 1.6, and 0.015 for M_0 greater than about 1.6.

The largest obtainable incremental thrust ratio for the shroud-length combinations $L_s/D_p = 0.21$, $L_t/D_p = 0.54$, and $L_s/D_p = 0.21$, $L_t/D_p = 0.90$ is plotted in figure 9 as a function of flight Mach number for both an auxiliary free-stream scoop and an auxiliary boundary-layer scoop. The incremental thrust-ratio curve for the ideal nozzle (from ref. 9) is presented for comparison. Within the limits of the assumptions in calculating incremental thrust ratio, the nature of the data (pressure rather than force), and the estimated accuracy of the incremental thrust ratios, values approaching those of the ideal nozzle seem obtainable by using the given double-shroud ejector over the Mach number range of 0.8 to 2.3. For $M_0 > 1.33$, the thrusts obtainable from the combination $L_s/D_p = 0.21$, $L_t/D_p = 0.54$ are inferior to those obtained from the combination

3006

$L_s/D_p = 0.21$, $L_t/D_p = 0.90$. It is thus implied that the tertiary-shroud length should be increased with increase in flight Mach number for maximum thrust. However, the incremental thrust ratios for the shroud-length combination $L_s/D_p = 0.21$, $L_t/D_p = 0.90$ are greater than the ideal-nozzle values over the range of Mach number considered. The thrusts obtainable by using a boundary-layer scoop are 2 to $4\frac{1}{2}$ percent (of convergent-nozzle thrust) smaller than those obtainable by using a normal-shock free-stream scoop.

3006

The secondary and tertiary flows must be independently controlled, since they have no common pressure when operating at best thrust conditions.

It was mentioned previously that thrusts larger than ideal-nozzle thrusts are obtainable. A calculation using heat-transfer coefficients from reference 10 indicates that, for $(\omega\sqrt{\tau})_s \approx 0.09$, an increase in fuel rate of about $1\frac{1}{2}$ percent is required in order to maintain the primary total temperature at 3900° R. The secondary cooling air acquires a portion of this heat energy and converts it into thrust. This added fuel is not considered in the case of the ideal nozzle, since the ideal-nozzle calculation does not involve cooling or heat transfer.

Pumping Characteristics at Take-Off

At take-off ($M_0 = 0$), the nozzle pressure ratio is equal to P_0/P_p; for a turbojet power plant, the nozzle pressure ratio is about 0.515 for a typical case. This value is also the maximum pressure ratio available to the secondary and tertiary at take-off, by assuming no total-pressure losses in the secondary- and tertiary-flow passages. By reference to figure 3, it is seen that this value corresponds to $(\omega\sqrt{\tau})_s$ and $(\omega\sqrt{\tau})_t$, which are between 0.03 and 0.06 for the pair of diameter ratios considered in this investigation. Thus, at take-off, the pumping characteristics of the ejector are sufficient to provide a nominal amount of cooling.

SUMMARY OF RESULTS

The following results were obtained from the present investigation of the flow characteristics and thrust performance of a double-cylindrical-shroud ejector:

1. Thrust performance on the order of that obtainable from an ideal nozzle may be obtained in the Mach number range of 0.8 to 2.3 when the

secondary flow is also used for afterburner cooling. Short secondary-shroud lengths are prescribed throughout, while an increase in tertiary-shroud length with increasing Mach number is indicated. Also high secondary and low tertiary weight flows (not necessarily zero) are desirable.

2. The level of obtainable thrust performance is greatly dependent on the over-all performance of the auxiliary air inlet.

3. Fair agreement is obtained when experimental pressure data are compared with values obtained from the double-shroud ejector theory presented herein. The assumption of relative independence of the secondary and tertiary processes is partially confirmed.

Lewis Flight Propulsion Laboratory
National Advisory Committee for Aeronautics
Cleveland, Ohio, September 3, 1953

APPENDIX A

SYMBOLS

The following symbols are used in this report:

A	area perpendicular to ejector axis
A_a	projected area in free-stream direction of auxiliary scoop
a	$\frac{A_s}{A_p}$
B	$\frac{A_{s,2} + A_2}{A_p}$
b	$\frac{A_t}{A_p}$
D	diameter
E	ratio of turbine-exit total pressure to compressor-entrance total pressure
$\left(\frac{F}{F^*}\right)_M$	impulse ratio, $\frac{1 + \gamma M^2}{M} \sqrt{\frac{1}{2(\gamma+1)\left(1 + \frac{\gamma-1}{2} M^2\right)}}$
F_n	net internal thrust
g	acceleration due to gravity
L	shroud length
L_t'	tertiary-shroud-length increment, $L_t - L_s$
$\left(\frac{L}{D_p}\right)_{cr}$	critical shroud-length ratio
M	Mach number
P	total pressure
p	static pressure

3006 CF-2

R	gas constant
r_b	pressure recovery of auxiliary boundary-layer scoop
r_{in}	pressure recovery of inlet
r_r	pressure recovery of auxiliary free-stream scoop
T	total temperature
t	static temperature
W	weight flow
α	$\frac{A_1}{A_p}$
β	$\frac{A_2}{A_p}$
γ	ratio of specific heats
τ	T/T_p
ν	Prandtl-Meyer angle
ω	W/W_p

Subscripts:

a	auxiliary scoop
b	boundary-layer scoop
c	convergent nozzle
cr	critical
e	ejector exit
i	ideal-nozzle value
in	inlet
is	isentropic

3006

[redacted]

m	miminum
p	primary, or station at exit of primary nozzle
r	ram scoop
s	secondary
t	tertiary
0	free stream
1	station at end of secondary shroud
2	station at end of tertiary shroud

Superscript:

*	sonic condition

3006

CF-2 back

[redacted]

APPENDIX B

APPROXIMATE THEORY FOR DOUBLE-CYLINDRICAL-SHROUD EJECTOR

An approximate theory based on that of reference 1 is presented herein. The assumptions in this theory are as follows: (1) The shroud lengths are sufficiently short that no mixing takes place between adjacent streams. (2) The primary expansion is isentropic in the cases involving secondary flow. (Where no secondary flow is involved, a free-jet expansion is obtained as the simultaneous solution of the conformity and momentum equations.) (3) The secondary flow and tertiary flow expand to sonic condition at the extremities of their respective shrouds. (4) In the case of tertiary flow, the secondary flow expands isentropically within the tertiary shroud.

3006

I. No Secondary Flow; No Tertiary Flow

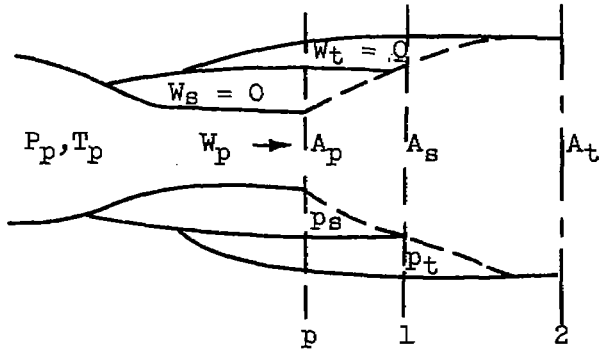

The one-dimensional continuity and momentum equations between stations p and 1 are considered. It is assumed that total temperature is conserved so that $T_p = T_1$, $P_s = p_1$, $p_t = P_2$, and also that the shroud lengths are greater than critical. The critical secondary-shroud length, as indicated in figure 5, is that beyond which there is negligible change in minimum secondary pressure ratio with an increase in secondary-shroud length. The continuity and momentum equations are

$$p_p M_p A_p \sqrt{1 + \frac{\gamma-1}{2} M_p^2} = p_1 M_1 A_s \sqrt{1 + \frac{\gamma-1}{2} M_1^2} \tag{B1}$$

$$p_p A_p (1 + \gamma M_p^2) + (A_s - A_p) p_1 = p_1 A_s (1 + \gamma M_1^2) \tag{B2}$$

By letting $a = \frac{A_s}{A_p}$ and solving (B1) and (B2) simultaneously,

$$a = \frac{\frac{M_p}{M_1}}{(1 + \gamma M_p^2)\sqrt{\frac{1 + \frac{\gamma-1}{2} M_1^2}{1 + \frac{\gamma-1}{2} M_p^2}} - \gamma M_1 M_p} \tag{B3}$$

and

$$\frac{p_1}{P_p} = \frac{1 + \gamma M_p^2}{\left(1 + \frac{\gamma-1}{2} M_p^2\right)^{\frac{\gamma}{\gamma-1}}} - \gamma M_1 M_p \sqrt{\frac{\left(1 + \frac{\gamma-1}{2} M_p^2\right)^{-\left(\frac{\gamma+1}{\gamma-1}\right)}}{1 + \frac{\gamma-1}{2} M_1^2}} \tag{B4}$$

But, in the primary expansion, M_p is assumed equal to unity. Therefore, (B3) and (B4) become

$$a = \frac{1}{M_1 \sqrt{2(1+\gamma)\left(1 + \frac{\gamma-1}{2} M_1^2\right) - \gamma M_1^2}} \tag{B3a}$$

and

$$\frac{p_1}{P_p} = \frac{1 + \gamma}{\left(\frac{\gamma+1}{2}\right)^{\frac{\gamma}{\gamma-1}}} - \gamma M_1 \left(\frac{2}{\gamma+1}\right)^{\frac{1}{2}\left(\frac{\gamma+1}{\gamma-1}\right)} \frac{1}{\sqrt{1 + \frac{\gamma-1}{2} M_1^2}}$$

or, in alternate form,

$$\frac{p_1}{P_p} = \frac{\left(\frac{2}{\gamma+1}\right)^{\frac{1}{2}\left(\frac{\gamma+1}{\gamma-1}\right)}}{aM_1 \sqrt{1 + \frac{\gamma-1}{2} M_1^2}} \tag{B4a}$$

3006

[redacted]

where a is determined for a given value of M_1 by equation (B3a).

The equations for the flow between stations 1 and 2 are identical to equations (B3) and (B4), except that subscript p is replaced by subscript 1, subscript 1 by 2, and a by b/a where $b = A_t/A_p$. These equations thus become

$$b = \frac{a\left(\frac{M_1}{M_2}\right)}{(1 + \gamma M_1^2)\sqrt{\frac{1 + \frac{\gamma-1}{2} M_2^2}{1 + \frac{\gamma-1}{2} M_1^2}} - \gamma M_1 M_2} \tag{B5}$$

and

$$\frac{p_2}{P_1} = \frac{a}{b} \frac{M_1}{M_2} \frac{\left(1 + \frac{\gamma-1}{2} M_1^2\right)^{-\frac{(\gamma+1)}{2(\gamma-1)}}}{\sqrt{1 + \frac{\gamma-1}{2} M_2^2}} \tag{B6}$$

but

$$\frac{P_1}{P_p} = \frac{\left(\frac{A}{A^*}\right)_{M_1,is}}{a}$$

$$\frac{p_2}{P_p} = \frac{\left(\frac{A}{A^*}\right)_{M_1}}{b} \left(\frac{M_1}{M_2}\right) \frac{\left(1 + \frac{\gamma-1}{2} M_1^2\right)^{-\frac{\gamma+1}{2(\gamma-1)}}}{\sqrt{1 + \frac{\gamma-1}{2} M_2^2}} \tag{B6a}$$

The method of solution is, therefore, as follows:

(1) M_1 is assumed.

(2) From equations (B3a) and (B4a), a and p_1/P_p are calculated, to give the variation of a and p_1/P_p with M_1.

(3) M_2 and desired values of a, M_1, and p_1/P_p are assumed.

(4) From equations (B5) and (B6a), b and p_2/P_p are calculated, to give the variation of b and p_2/P_p with M_2 for the assumed secondary conditions.

For shroud lengths smaller than $\left(\frac{L}{D_p}\right)_{cr}$, approximate values of p_1/P_p and p_2/P_p can be obtained by assuming that the primary fluid undergoes a Prandtl-Meyer expansion so that the fluid just strikes the shroud extremity. Therefore,

3006

$$\nu_s = \tan^{-1} \frac{\left(\frac{D_s}{D_p}\right) - 1}{2\left(\frac{L_s}{D_p}\right)} \tag{B7}$$

and

$$\nu_t - \nu_{M_1} = \tan^{-1} \frac{\left(\frac{D_t}{D_s}\right) - 1}{2\left(\frac{L_t'}{D_s}\right)} = \tan^{-1} \frac{\left(\frac{D_t}{D_p}\right) - \left(\frac{D_s}{D_p}\right)}{2\left(\frac{L_t'}{D_p}\right)} \tag{B8}$$

Equation (B7) can also be used for the tertiary shroud when the secondary shroud is shorter than $(L/D_p)_{cr}$. In that case, the pressure ratio corresponds directly to ν as read in tables of Prandtl-Meyer flow. Equation (B8) is used when $\frac{L_s}{D_p} > \left(\frac{L_s}{D_p}\right)_{cr}$ but $\left(\frac{L_t'}{D_s}\right) < \left(\frac{L_t'}{D_s}\right)_{cr}$. In that case,

$$\frac{p_2}{P_p} = \left(\frac{p}{P}\right)_{\nu_t} \frac{\left(\frac{A}{A^*}\right)_{M_1}}{a} \tag{B9}$$

The calculation is only approximate, since a three-dimensional effect is being calculated by a two-dimensional method.

II. Secondary Flow; No Tertiary Flow

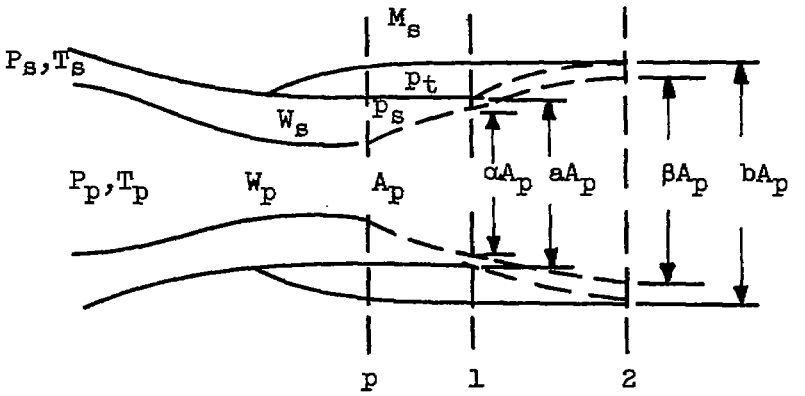

For the case of secondary flow and no tertiary flow and for further cases, it is assumed that there is no mixing of the various flows. It is also assumed that the secondary flow becomes sonic at station 1, that the primary flow is always isentropic, and that there is no energy interchange, so that $T_p = T_{p,1} = T_{p,2}$ and $T_s = T_{s,1} = T_{s,2}$.

The equations for primary and secondary continuity between stations p and 1 are, respectively,

$$\sqrt{\frac{R}{\gamma g}}\ \frac{W_p\sqrt{T_p}}{A_p} = p_p\sqrt{\frac{\gamma+1}{2}} = \alpha p_1 M_1\sqrt{1+\frac{\gamma-1}{2}M_1^2} \tag{B10}$$

and

$$\sqrt{\frac{R}{\gamma g}}\frac{W_s\sqrt{T_s}}{A_p} = p_s M_s(a-1)\sqrt{1+\frac{\gamma-1}{2}M_s^2} = p_1(a-\alpha)\sqrt{\frac{\gamma+1}{2}} \tag{B11}$$

where

$$\alpha = \left(\frac{A}{A^*}\right)_{M_1} = \frac{1}{M_1}\left[\frac{2\left(1+\frac{\gamma-1}{2}M_1^2\right)}{\gamma+1}\right]^{\frac{1}{2}\left(\frac{\gamma+1}{\gamma-1}\right)}$$

$$(\omega\sqrt{\tau})_s = \frac{W_s\sqrt{T_s}}{W_p\sqrt{T_p}} = \left(\frac{p_s}{p_p}\right)\frac{M_s(a-1)}{\sqrt{\frac{\gamma+1}{2}}}\sqrt{1+\frac{\gamma-1}{2}M_s^2}$$

3006

$$\left(\frac{P_s}{P_p}\right)_m = \frac{(\omega\sqrt{\tau})_s}{(a-1)} \left(\frac{A}{A^*}\right)_{M_s} \tag{B12}$$

The expression for conservation of momentum between stations p and 1 is written:

$$p_p(1 + \gamma) + (a - 1)p_s(1 + \gamma M_s^2) = p_1(a - \alpha)(1 + \gamma) + p_1\alpha(1 + \gamma M_1^2) \tag{B13}$$

By using relations (B10) and (B11), equation (B13) can be written

$$(\omega\sqrt{\tau})_s = \frac{\left(\frac{F}{F^*}\right)_{M_1} - 1}{\left(\frac{F}{F^*}\right)_{M_s} - 1} \tag{B14}$$

where $(F/F^*)_M = \frac{1 + \gamma M^2}{M} \sqrt{\frac{1}{2(\gamma+1)\left(1 + \frac{\gamma-1}{2} M^2\right)}}$. Tables of F/F^* as a function of Mach number are found in reference 11.

Between stations 1 and 2, the equations of primary and secondary continuity are

$$\sqrt{\frac{R}{\gamma g}} \frac{W_p \sqrt{T_p}}{A_p} = p_p \sqrt{\frac{\gamma+1}{2}} = p_1\alpha M_1 \sqrt{1 + \frac{\gamma-1}{2} M_1^2} = p_2\beta M_2 \sqrt{1 + \frac{\gamma-1}{2} M_2^2} \tag{B15}$$

$$\sqrt{\frac{R}{\gamma g}} \frac{W_s \sqrt{T_s}}{A_p} = p_1(a-\alpha) \sqrt{\frac{\gamma+1}{2}} = p_2 M_{s,2}(b-\beta) \sqrt{1 + \frac{\gamma-1}{2} M_{s,2}^2} \tag{B16}$$

and the expression for conservation of momentum is

$$p_1\alpha(1 + \gamma M_1^2) + p_1(a - \alpha)(1 + \gamma) + p_t(b - a)$$

$$= p_2\beta(1 + \gamma M_2^2) + p_2(b - \beta)(1 + \gamma M_{s,2}^2) \tag{B17}$$

The static pressure at the tertiary shroud p_t is taken equal to p_2 and $p_{s,2}$, since this pressure applies all along the free boundary and the calculation is made for the case of the secondary flow just attaching to the end of the tertiary shroud. Thus,

3006

CF-3

$$(b-a) = \frac{p_1}{p_2}\left\{\alpha(1 + \gamma M_1^2)\left[\frac{\left(\frac{F}{F^*}\right)_{M_2}}{\left(\frac{F}{F^*}\right)_{M_1}} - 1\right] + (a-\alpha)(1+\gamma)\left[(F/F^*)_{M_{s,2}} - 1\right]\right\} \tag{B18}$$

$$\frac{p_1}{p_2} = \left[\frac{1 + \frac{\gamma-1}{2} M_2^2}{1 + \frac{\gamma-1}{2} M_1^2}\right]^{\frac{\gamma}{\gamma-1}} \tag{B19}$$

3006

and, from the secondary continuity equation,

$$M_{s,2}\sqrt{1 + \frac{\gamma-1}{2} M_{s,2}^2} = \left(\frac{a-\alpha}{b-\beta}\right)\left(\frac{p_1}{p_2}\right) \tag{B20}$$

Since a, α, M_1, p_1/P_p, and $(F/F^*)_{M,1}$ are known from the first part of the solution of this case, the method of procedure is as follows for a fixed value of b:

(1) M_2 is assumed. After p_2/P_p and β are determined, then p_1/p_2 and the quantity $M_{s,2}\sqrt{1 + \frac{\gamma-1}{2} M_{s,2}^2}$ are calculated from equation (B20).

(2) Next, $M_{s,2}$ is calculated; then, $(F/F^*)_{M_{s,2}}$ is determined and $(F/F^*)_{M_2}$ is calculated from the following form of equation (B18):

$$\left(\frac{F}{F^*}\right)_{M_2} = \left(\frac{F}{F^*}\right)_{M_1}\left\{1 + \frac{\frac{p_2}{p_1}(b-a) - (a-\alpha)(1+\gamma)\left[\left(\frac{F}{F^*}\right)_{M_{s,2}} - 1\right]}{\alpha(1 + \gamma M_1^2)}\right\} \tag{B21}$$

(3) Then M_2 is determined and checked with the initial assumption.

[redacted]

2006

CF-3 back

III. No Secondary Flow; Tertiary Flow

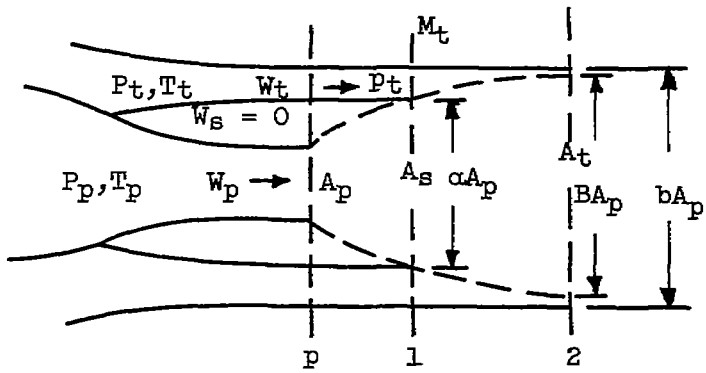

The solution between stations p and 1 is the same as that of part I. The continuity relations for the primary and tertiary flow are written

$$\sqrt{\frac{R}{\gamma g}}\frac{W_p\sqrt{T_p}}{A_p} = p_p\sqrt{\frac{\gamma+1}{2}} = ap_1M_1\sqrt{1+\frac{\gamma-1}{2}M_1^2} = Bp_2M_2\sqrt{1+\frac{\gamma-1}{2}M_2^2} \tag{B22}$$

and

$$\sqrt{\frac{R}{\gamma g}}\frac{W_t\sqrt{T_t}}{A_p} = (b-a)p_tM_t\sqrt{1+\frac{\gamma-1}{2}M_t^2} = (b-B)p_2\sqrt{\frac{\gamma+1}{2}} \tag{B23}$$

The momentum relation between stations 1 and 2 is written

$$ap_1(1+\gamma M_1^2) + (b-a)p_t(1+\gamma M_t^2) = Bp_2(1+\gamma M_2^2) + (b-B)p_2(1+\gamma) \tag{B24}$$

Solution of equations (B22), (B23), and (B24) yields

$$B = a\frac{\left(\frac{A}{A^*}\right)_{M_2}}{\left(\frac{A}{A^*}\right)_{M_1}} \tag{B25}$$

$$(\omega\sqrt{\tau})_t = \left(\frac{\gamma+1}{2}\right)^{\frac{\gamma}{\gamma-1}} \frac{p_1}{p_p} (b-B) \frac{\left(\frac{p_2}{p_2}\right)_{M_2}}{\left(\frac{p_1}{p_1}\right)_{M_1}} \tag{B26}$$

$$\left(\frac{F}{F^*}\right)_{M_t} = 1 + \frac{\left(\frac{F}{F^*}\right)_{M_2} - \left(\frac{F}{F^*}\right)_{M_1}}{(\omega\sqrt{\tau})_t} \tag{B27}$$

3006

and

$$\left(\frac{P_t}{P_p}\right)_m = \frac{(\omega\sqrt{\tau})_t \left(\frac{A}{A^*}\right)_{M_t}}{(b-a)} \tag{B28}$$

The method of calculation between stations 1 and 2 is as follows:

(1) M_2 is assumed, and B is then calculated from equation (B25).

(2) From equation (B26), $(\omega\sqrt{\tau})_t$ is calculated.

(3) The values of $(F/F^*)_{M_1}$ and $(F/F^*)_{M_2}$ are determined. Then $(F/F^*)_{M_t}$ is calculated from equation (B27). The value of M_t is obtained from tables of (F/F^*).

(4) The value of $(A/A^*)_{M_t}$ is obtained from isentropic-flow tables. Then $(P_t/P_p)_m$ is calculated from equation (B28).

IV. Secondary and Tertiary Flow

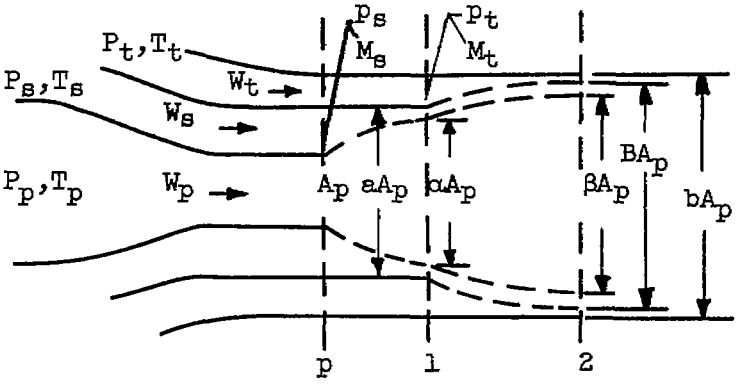

The solution with both secondary and tertiary flow between stations p and 1 is the same as that of part II. The continuity relations for primary, secondary, and tertiary flows are as follows:

$$\sqrt{\frac{R}{\gamma g}}\frac{W_p\sqrt{T_p}}{A_p} = p_p\sqrt{\frac{\gamma+1}{2}} = \alpha p_1 M_1\sqrt{1+\frac{\gamma-1}{2}M_1^2} = \beta p_2 M_2\sqrt{1+\frac{\gamma-1}{2}M_2^2} \tag{B29}$$

$$\sqrt{\frac{R}{\gamma g}}\frac{W_s\sqrt{T_s}}{A_p} = (a-1)p_s M_s\sqrt{1+\frac{\gamma-1}{2}M_s^2} = (a-\alpha)p_1\sqrt{\frac{\gamma+1}{2}}$$

$$= (B-\beta)p_2 M_{s,2}\sqrt{1+\frac{\gamma-1}{2}M_{s,2}^2} \tag{B30}$$

and

$$\sqrt{\frac{R}{\gamma g}}\frac{W_t\sqrt{T_t}}{A_p} = (b-a)p_t M_t\sqrt{1+\frac{\gamma-1}{2}M_t^2} = (b-B)p_2\sqrt{\frac{\gamma+1}{2}} \tag{B31}$$

It is assumed that $M_{t,2} = 1$. Also, it is assumed that the primary and secondary flows between stations 1 and 2 are isentropic. The momentum relation between stations 1 and 2 is

$$p_1\alpha(1+\gamma M_1^2) + p_1(a-\alpha)(1+\gamma) + p_t(b-a)(1+\gamma M_t^2)$$

$$= p_2\beta(1+\gamma M_2^2) + p_2(B-\beta)(1+\gamma M_{s,2}^2) + p_2(b-B)(1+\gamma) \tag{B32}$$

From the assumption of isentropic primary and secondary flows between stations 1 and 2 and the assumptions $p_{s,2} = p_2$, $p_{s,1} = p_1$, $M_{s,1} = 1$, the following relation is obtained:

$$1+\frac{\gamma-1}{2}M_{s,2}^2 = \left(\frac{\gamma+1}{2}\right)\left(\frac{1+\frac{\gamma-1}{2}M_2^2}{1+\frac{\gamma-1}{2}M_1^2}\right) \tag{B33}$$

From solution of equations (B29) through (B32), the following values are obtained:

$$(B-\beta) = (a-\alpha)\left(\frac{A}{A^*}\right)_{M_{s,2}} \tag{B34}$$

$$(\omega\sqrt{\tau})_t = (b-B)\,\frac{p_2}{p_p}\left(\frac{\gamma+1}{2}\right)^{\frac{\gamma}{\gamma-1}} \tag{B35}$$

$$\left(\frac{F}{F^*}\right)_{M_t} = 1 + \frac{(\omega\sqrt{\tau})_s\left[\left(\frac{F}{F^*}\right)_{M_{s,2}} - 1\right] + \left(\frac{F}{F^*}\right)_{M_2} - \left(\frac{F}{F^*}\right)_{M_1}}{(\omega\sqrt{\tau})_t} \tag{B36}$$

$$\left(\frac{P_t}{P_p}\right)_m = \frac{(\omega\sqrt{\tau})_t}{(b-a)}\left(\frac{A}{A^*}\right)_t \tag{B37}$$

3006

The known quantities between stations 1 and 2 are a, α, M_1, and $(\omega\sqrt{\tau})_s$, as determined from part II. The method of calculation is as follows:

(1) M_2 is assumed, and $M_{s,2}$ is calculated from equation (B33). From isentropic-flow tables, $\beta = (A/A^*)_{M,2}$ and p_2/P_p are calculated.

(2) From equation (B34), $(B - \beta)$ is calculated.

(3) Then b is assumed, and $(\omega\sqrt{\tau})_t$ is calculated from equation (B35).

(4) From equation (B36), $(F/F^*)_{M_t}$ is calculated.

(5) Then M_t is determined, and $(A/A^*)_{M_t}$ is calculated.

(6) From equation (B37), $(P_t/P_p)_m$ is calculated.

[redacted]

3006

APPENDIX C

CALCULATION OF NET INTERNAL THRUST FOR DOUBLE-CYLINDRICAL-SHROUD EJECTOR - INCREMENTAL THRUST RATIO

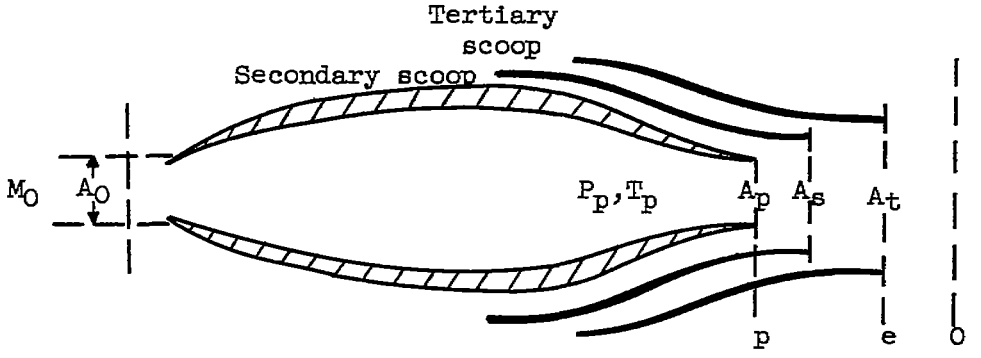

From momentum considerations, the net internal thrust for a double-cylindrical-shroud ejector can be written

$$F_n = A_p p_p(1 + \gamma M_p^2) + (A_s - A_p)p_s\,(1 + \gamma M_s^2) + (A_t - A_s)p_t\,(1 + \gamma M_t^2) - A_0 p_0(1 + \gamma M_0^2) + p_0(A_0 - A_t) - (A_{a,s} + A_{a,t})\gamma p_0 M_0^2 \qquad (C1)$$

This expression is made dimensionless through division by $A_p P_p$:

$$\frac{F_n}{A_p P_p} = \frac{1 + \gamma M_p^2}{\left(1 + \frac{\gamma-1}{2} M_p^2\right)^{\frac{\gamma}{\gamma-1}}} + (a-1)\,\frac{P_s}{P_p}\,\frac{1 + \gamma M_s^2}{\left(1 + \frac{\gamma-1}{2} M_s^2\right)^{\frac{\gamma}{\gamma-1}}} + (b-a)\,\frac{P_t}{P_p}\,\frac{1 + \gamma M_t^2}{\left(1 + \frac{\gamma-1}{2} M_t^2\right)^{\frac{\gamma}{\gamma-1}}} - \frac{A_0}{A_p}\,\frac{p_0}{P_p}\,\gamma M_0^2 - \frac{p_0}{P_p}\,b - \left(\frac{A_{a,s} + A_{a,t}}{A_p}\right)\gamma\,\frac{p_0}{P_p}\,M_0^2 \qquad (C2)$$

By assuming choked flow in the convergent nozzle, $M_p = 1$. Also, the expression for the ideal net thrust of a choked convergent nozzle (from ref. 9, appendix C) is the following:

[redacted]

$$\frac{(F_n)_{c,i}}{A_p P_p} = (1+\gamma)\left(\frac{2}{\gamma+1}\right)^{\frac{\gamma}{\gamma-1}} - \frac{A_0}{A_p}\frac{p_0}{P_p}\gamma M_0^2 - \frac{p_0}{P_p}$$

$$= \left[(1+\gamma)\left(\frac{2}{\gamma+1}\right)^{\frac{\gamma}{\gamma-1}}\right]\left[1 - \frac{\gamma M_0}{\sqrt{2(\gamma+1)}}\sqrt{\frac{t_0}{T_p}}\right] - \frac{p_0}{P_p} \quad (C3)$$

Thus, the incremental thrust ratio is written

$$\frac{F_n - (F_n)_{c,i}}{(F_n)_{c,i}} = \frac{(a-1)\frac{P_s}{P_p}\frac{1+\gamma M_s^2}{\left(1+\frac{\gamma-1}{2}M_s^2\right)^{\frac{\gamma}{\gamma-1}}} + (b-a)\frac{P_t}{P_p}\frac{1+\gamma M_t^2}{\left(1+\frac{\gamma-1}{2}M_t^2\right)^{\frac{\gamma}{\gamma-1}}} - (b-1)\frac{p_0}{P_p} - \left(\frac{A_{a,s}+A_{a,t}}{A_p}\right)\frac{p_0}{P_p}\gamma M_0^2}{\left[(1+\gamma)\left(\frac{2}{\gamma+1}\right)^{\frac{\gamma}{\gamma-1}}\right]\left[1 - \frac{\gamma M_0}{\sqrt{2(\gamma+1)}}\sqrt{\frac{t_0}{T_p}}\right] - \frac{p_0}{P_p}} \quad (C4)$$

From mass-flow considerations,

$$A_{a,s} = \frac{W_s}{W_p}A_0 = \left[\frac{W_s}{W_p}\sqrt{\frac{T_s}{T_p}}\right]\sqrt{\frac{T_p}{T_s}}A_0 = (\omega\sqrt{\tau})_s\sqrt{\frac{T_p}{T_s}}A_0$$

and

$$A_{a,t} = (\omega\sqrt{\tau})_t\sqrt{\frac{T_p}{T_t}}A_0$$

Therefore,

$$\left(\frac{A_{a,s}+A_{a,t}}{A_p}\right)\frac{p_0}{P_p}\gamma M_0^2 = \frac{A_0}{A_p}\frac{p_0}{P_p}\gamma M_0^2\left[(\omega\sqrt{\tau})_s\sqrt{\frac{T_p}{T_s}} + (\omega\sqrt{\tau})_t\sqrt{\frac{T_p}{T_t}}\right]$$

but, from continuity between stations 0 and p,

$$\frac{A_0}{A_p} = \frac{1}{M_0}\frac{P_p}{p_0}\sqrt{\frac{T_0}{T_p}}\frac{\left(\frac{2}{\gamma+1}\right)^{\frac{\gamma+1}{2(\gamma-1)}}}{\sqrt{1+\frac{\gamma-1}{2}M_0^2}}$$

3006

[redacted]

Thus,

$$\left(\frac{A_{a,s} + A_{a,t}}{A_p}\right)\frac{p_0}{P_p}\gamma M_0^2 = \frac{\left(\frac{2}{\gamma+1}\right)^{\frac{\gamma+1}{2(\gamma-1)}}\gamma M_0}{\sqrt{1 + \frac{\gamma-1}{2}M_0^2}}\left[(\omega\sqrt{\tau})_s\sqrt{\frac{T_0}{T_s}} + (\omega\sqrt{\tau})_t\sqrt{\frac{T_0}{T_t}}\right]$$

Equation (C4) then becomes:

$$\frac{F_n - (F_n)_{c,i}}{(F_n)_{o,i}} = \frac{(a-1)\frac{P_s}{P_p}\left[\frac{1+\gamma M_s^2}{\left(1+\frac{\gamma-1}{2}M_s^2\right)^{\frac{1}{\gamma-1}}}\right] + (b-a)\frac{P_t}{P_p}\left[\frac{1+\gamma M_t^2}{\left(1+\frac{\gamma-1}{2}M_t^2\right)^{\frac{1}{\gamma-1}}}\right] - (b-1)\frac{p_0}{P_p} - \frac{\gamma M_0}{\sqrt{1+\frac{\gamma-1}{2}M_0^2}}\left(\frac{2}{\gamma+1}\right)^{\frac{\gamma+1}{2(\gamma-1)}}\sum_{s,t}\left[(\omega\sqrt{\tau})\sqrt{\frac{T_0}{T}}\right]}{\left[(1+\gamma)\left(\frac{2}{\gamma+1}\right)^{\frac{1}{\gamma-1}}\right]\left[1 - \frac{\gamma M_0}{\sqrt{2(\gamma+1)}}\sqrt{\frac{T_0}{T_p}}\right] - \frac{p_0}{P_p}} \quad \text{(C5)}$$

The Mach numbers M_s and M_t are found from their respective area ratios by using the following derived relations:

$$\left(\frac{A}{A^*}\right)_{M_s} = \frac{(a-1)}{(\omega\sqrt{\tau})_s}\left(\frac{P_s}{P_p}\right) \quad \text{(B12a)}$$

and

$$\left(\frac{A}{A^*}\right)_{M_t} = \frac{(b-a)}{(\omega\sqrt{\tau})_t}\left(\frac{P_t}{P_p}\right) \quad \text{(B37a)}$$

where

$$\frac{A}{A^*} = \frac{1}{M}\left[\frac{2\left(1 + \frac{\gamma-1}{2}M^2\right)}{\gamma+1}\right]^{\frac{\gamma+1}{2(\gamma-1)}}$$

[redacted]

APPENDIX D

FLIGHT-PLAN ASSUMPTIONS

The schedule of engine pressure ratio E, inlet recovery r_{in}, ram-scoop recovery r_r, and boundary-layer scoop recovery r_b for the assumed turbojet flight plan is listed in the following table:

M_O	E	r_{in}	r_r	r_b	Altitude	T_p
0.8	2.169	0.96	1.00	0.87	Tropopause $t_O = 392^\circ$ R	3900° R
1.1	2.021	0.95	1.00	0.79		
1.4	1.846	0.925	0.95	0.685		
1.7	1.662	0.89	0.86	0.56		
2.0	1.474	0.85	0.72	0.43		
2.3	1.299	0.81	0.59	0.32		

Nozzle pressure ratio p_O/P_p is determined as follows:

$$\frac{p_O}{P_p} = \frac{p_O}{P_O Er_{in}} = \frac{1}{Er_{in}\left(1 + \frac{\gamma-1}{2} M_O^2\right)^{\frac{\gamma}{\gamma-1}}} \tag{D1}$$

The maximum available pressure ratios used in connection with figures 8 and 9 are obtained from the following relations:

$$\left(\frac{P_s}{P_p}\right)_{max} = \frac{r_r}{Er_{in}} \tag{D2a}$$

$$\left(\frac{P_s}{P_p}\right)_{max} = \frac{r_b}{Er_{in}} \tag{D2b}$$

Equation (D2a) applies to the use of an auxiliary ram scoop, while equation (D2b) applies to the use of an auxiliary boundary-layer scoop. These quantities, calculated by using the representative values in the preceding table, are plotted in figure 7.

3008

REFERENCES

1. Kochendorfer, Fred D., and Rousso, Morris D.: Performance Characteristics of Aircraft Cooling Ejectors Having Short Cylindrical Shrouds. NACA RM E51E01, 1951.

2. Greathouse, W. K., and Hollister, D. P.: Preliminary Air-Flow and Thrust Calibrations of Several Conical Cooling-Air Ejectors with a Primary to Secondary Temperature Ratio of 1.0. I - Diameter Ratios of 1.21 and 1.10. NACA RM E52E21, 1952.

3. Greathouse, W. K., and Hollister, D. P.: Preliminary Air-Flow and Thrust Calibrations of Several Conical Cooling-Air Ejectors with a Primary to Secondary Temperature Ratio of 1.0. II - Diameter Ratios of 1.06 and 1.40. NACA RM E52F26, 1952.

4. Greathouse, W. K., and Hollister, D. P.: Air-Flow and Thrust Characteristics of Several Cylindrical Cooling-Air Ejectors with a Primary to Secondary Temperature Ratio of 1.0. NACA RM E52L24, 1953.

5. Ellis, C. W., Hollister, D. P., and Wilsted, H. D.: Investigation of Performance of Several Double-Shroud Ejectors and Effect of Variable-Area Exhaust Nozzle on Single Ejector Performance. NACA RM E52D25, 1952.

6. Hollister, Donald P., and Greathouse, William K.: Performance of Double-Shroud Ejector Configuration with Primary Pressure Ratios from 1.0 to 10. NACA RM E52K17, 1953.

7. Burgess, Warren C., Jr., and Seashore, Ferris L.: Criterions for Condensation-Free Flow in Supersonic Tunnels. NACA TN 2518, 1951. (Supersedes NACA RM E9E02.)

8. Samuels, John C., and Yanowitz, Herbert: Analysis of Several Methods of Pumping Cooling Air for Turbojet-Engine Afterburners. NACA RM E52K26, 1953.

9. Reshotko, Eli: Preliminary Investigation of a Perforated Axially Symmetric Nozzle for Varying Nozzle Pressure Ratios. NACA RM E52J27, 1953.

10. Koffel, William K., and Kaufman, Harold R.: Investigation of Heat-Transfer Coefficients in an Afterburner. NACA RM E52D11, 1952.

11. Keenan, Joseph H., and Kaye, Joseph: Gas Tables. John Wiley & Sons, Inc., 1948.

3006

CF-4 back

[redacted]

TABLE I. - SHROUD-LENGTH COMBINATIONS TESTED

Secondary-shroud-length ratio, L_s/D_p	Tertiary-shroud-length ratio, L_t/D_p, at -				
	Tertiary-shroud-length-increment ratio, L_t'/D_p				
	0.16	0.33	0.50	0.69	0.86
0.11	0.27	0.44			
.21	.37	.54	0.72	0.90	1.07
.31		.64			
.41		.74			
.51		.84			

NACA

3006

3006

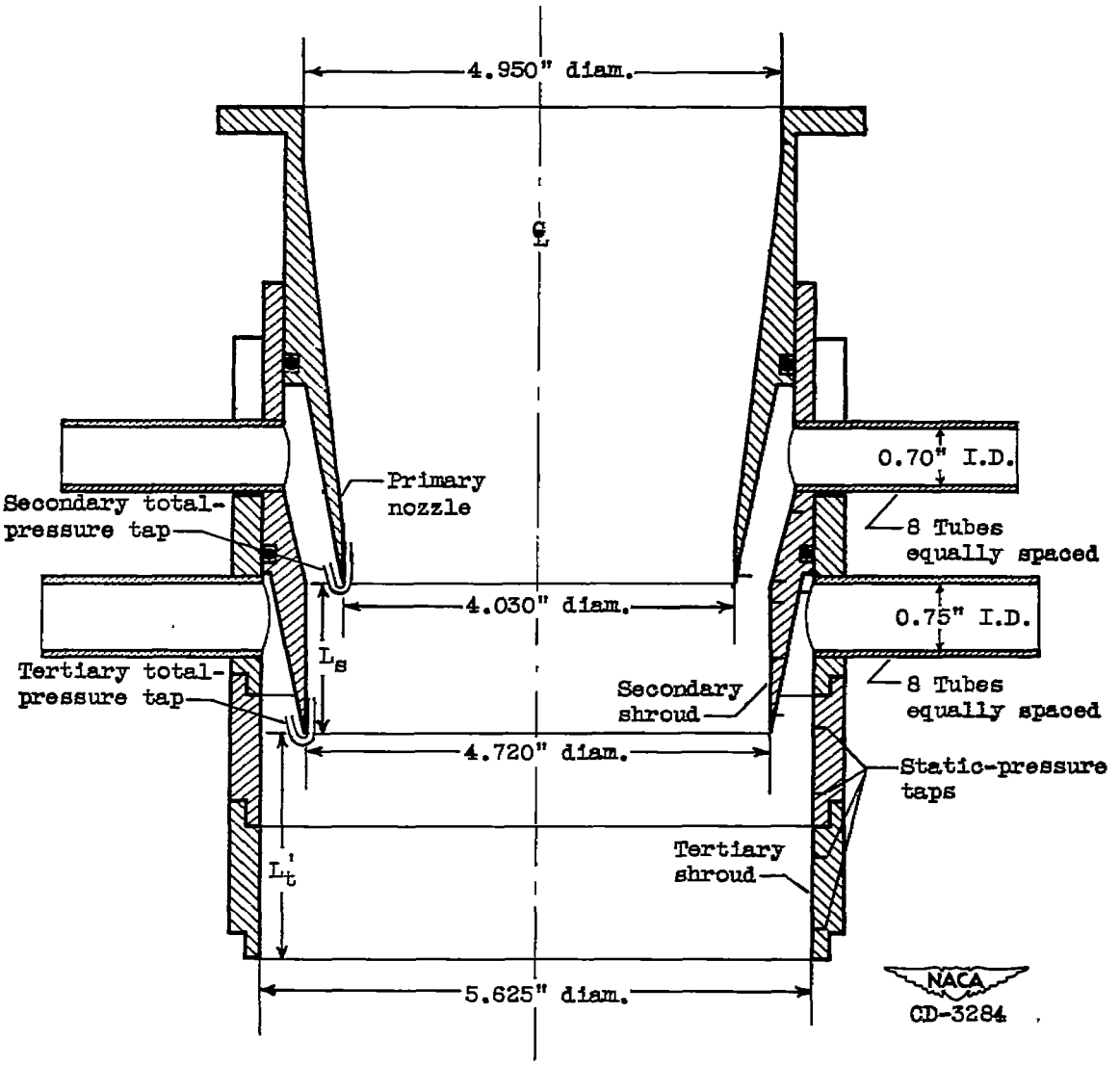

Figure 1. - Details of double-shroud ejector. ($L_t = L_s + L_t'$).

3006

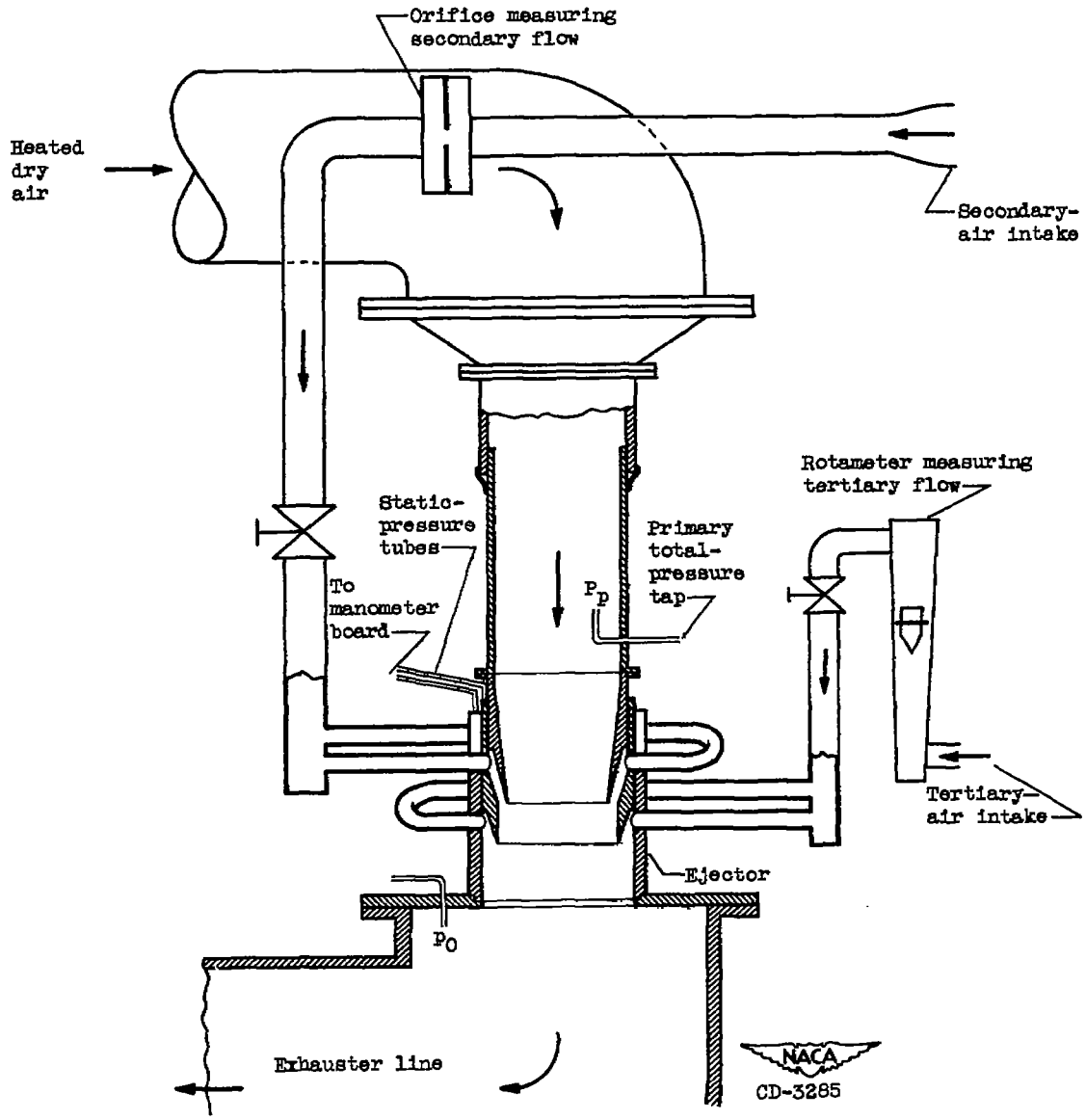

Figure 2. - Test setup

3006

3006

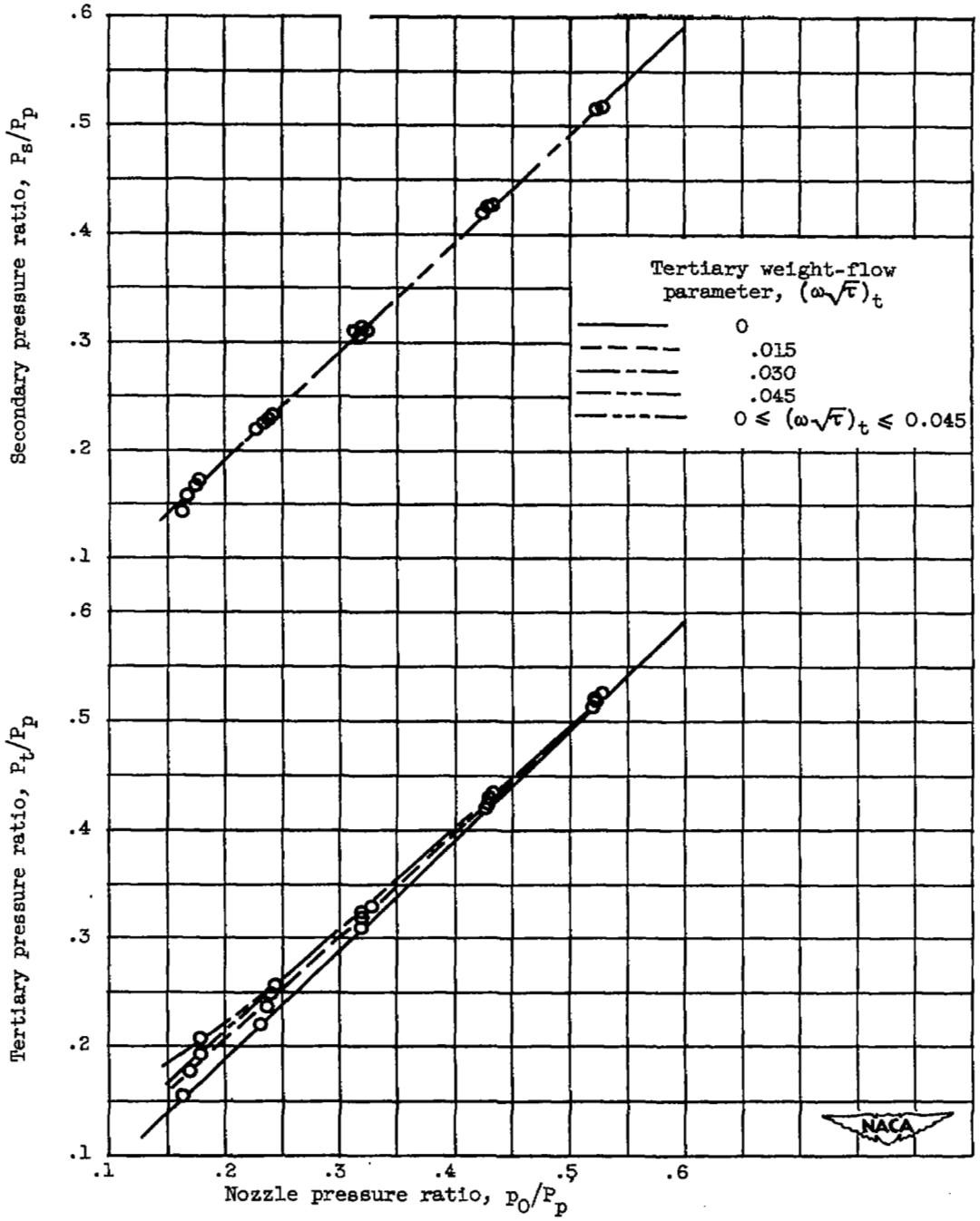

(a) Secondary-shroud-length ratio, 0.11; tertiary-shroud-length ratio, 0.27; secondary weight-flow parameter, 0.

Figure 3. - Ejector performance curves.

[redacted]

3006

CF-5

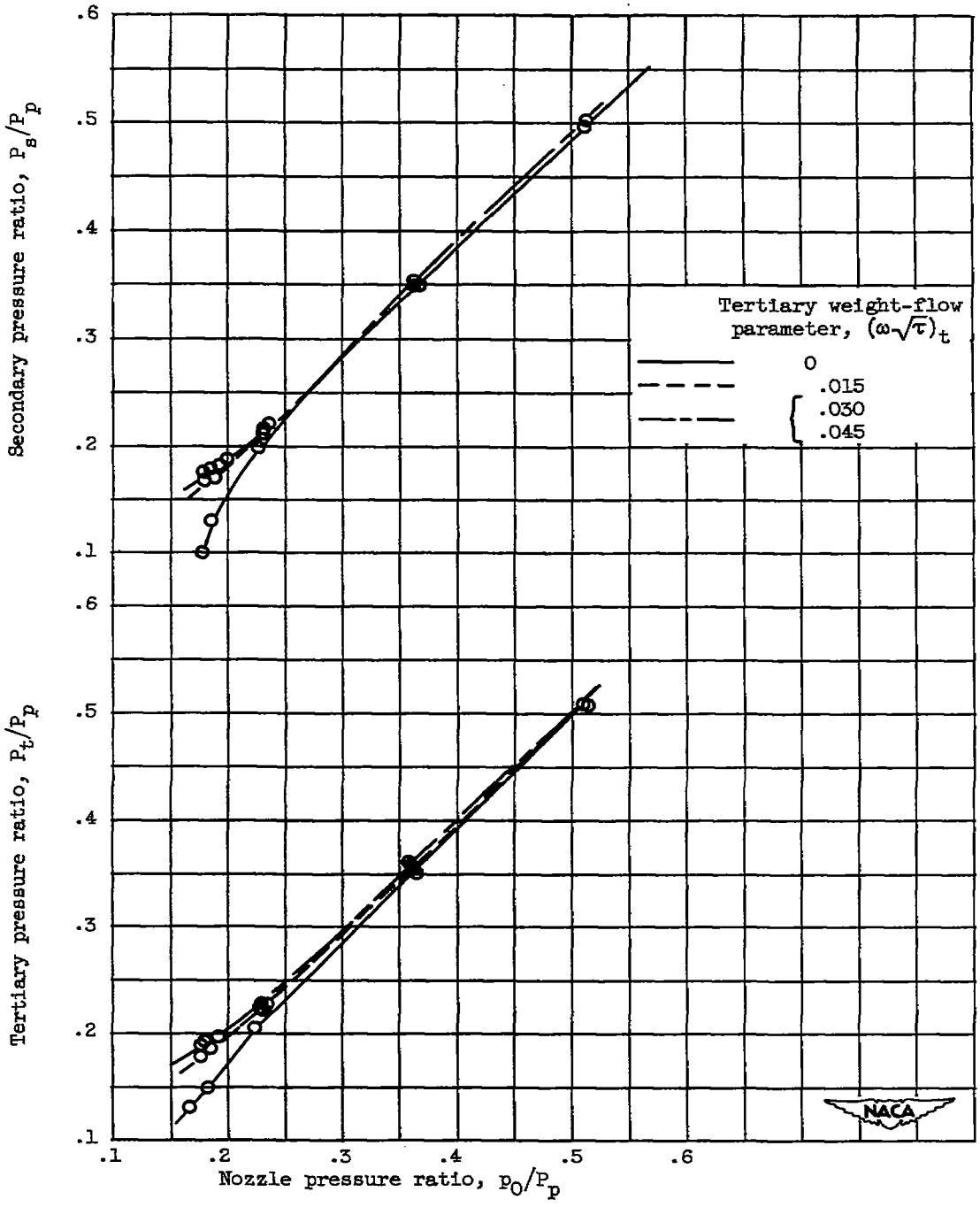

(b) Secondary-shroud-length ratio, 0.11; tertiary-shroud-length ratio, 0.44; secondary weight-flow parameter, 0.

Figure 3. - Continued. Ejector performance curves.

[redacted]

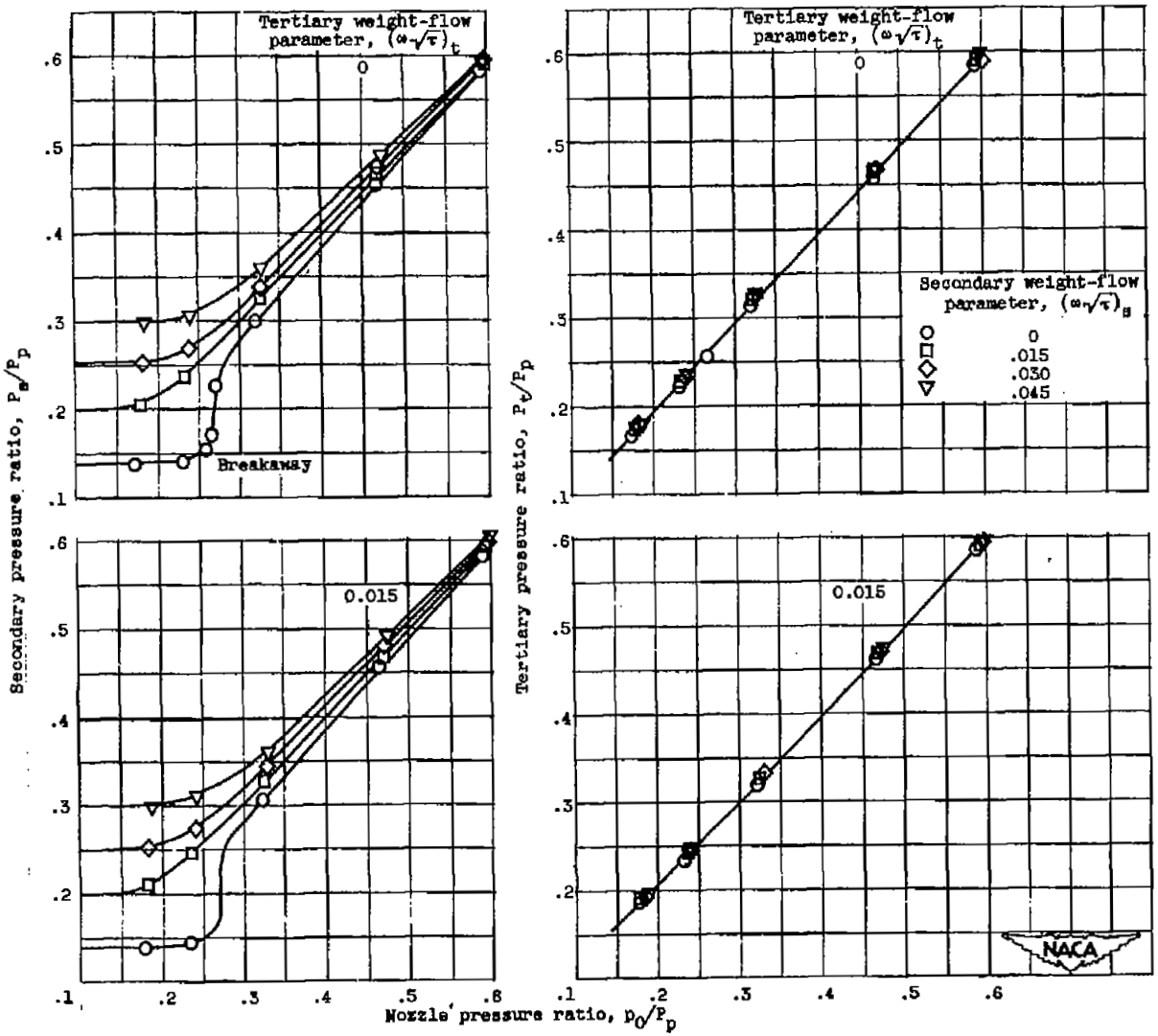

(c) Secondary-shroud-length ratio, 0.21; tertiary-shroud-length ratio, 0.57.

Figure 3. - Continued. Ejector performance curves.

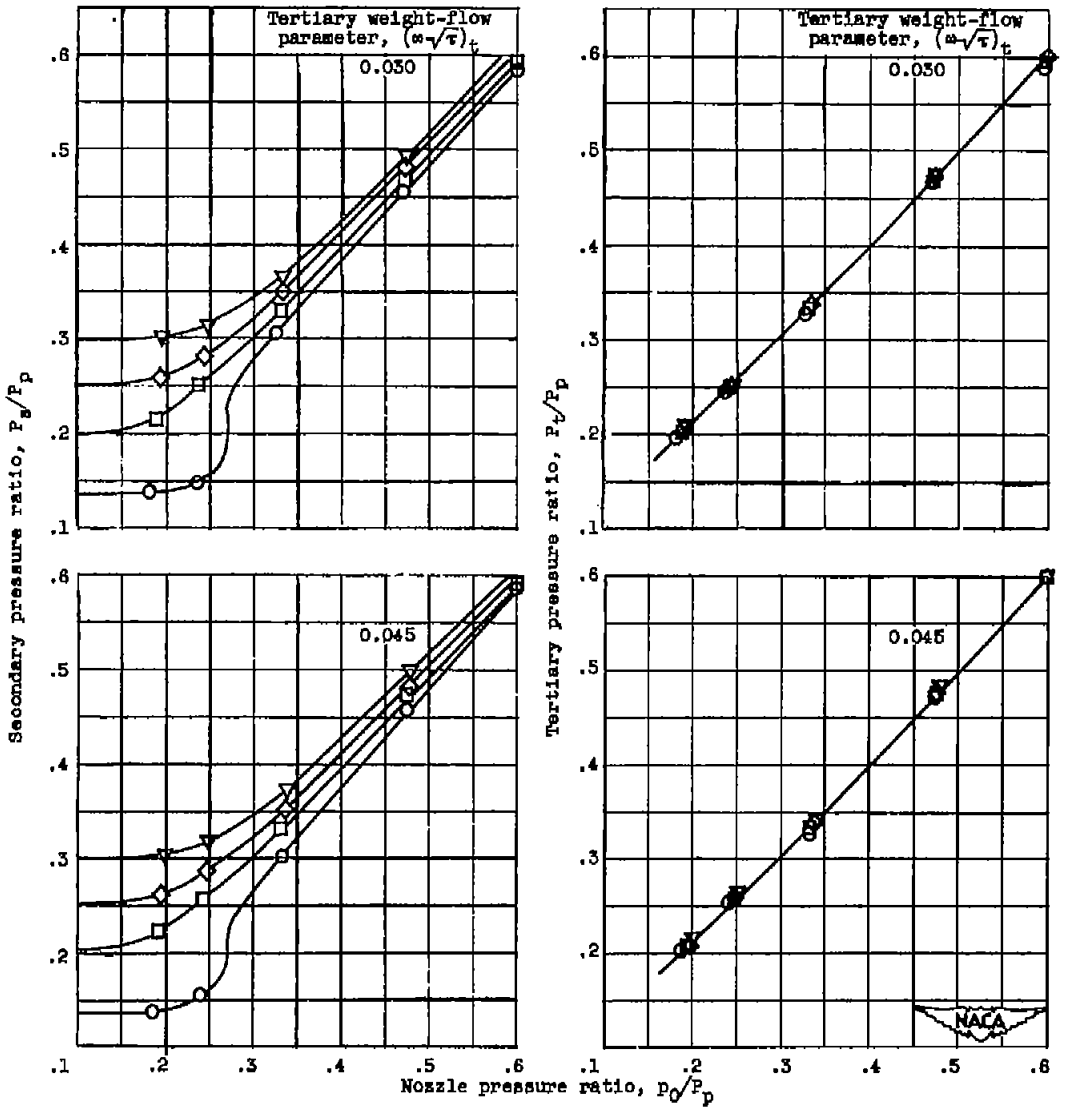

(c) Concluded. Secondary-shroud-length ratio, 0.21; tertiary-shroud-length ratio, 0.37.

Figure 3. - Continued. Ejector performance curves.

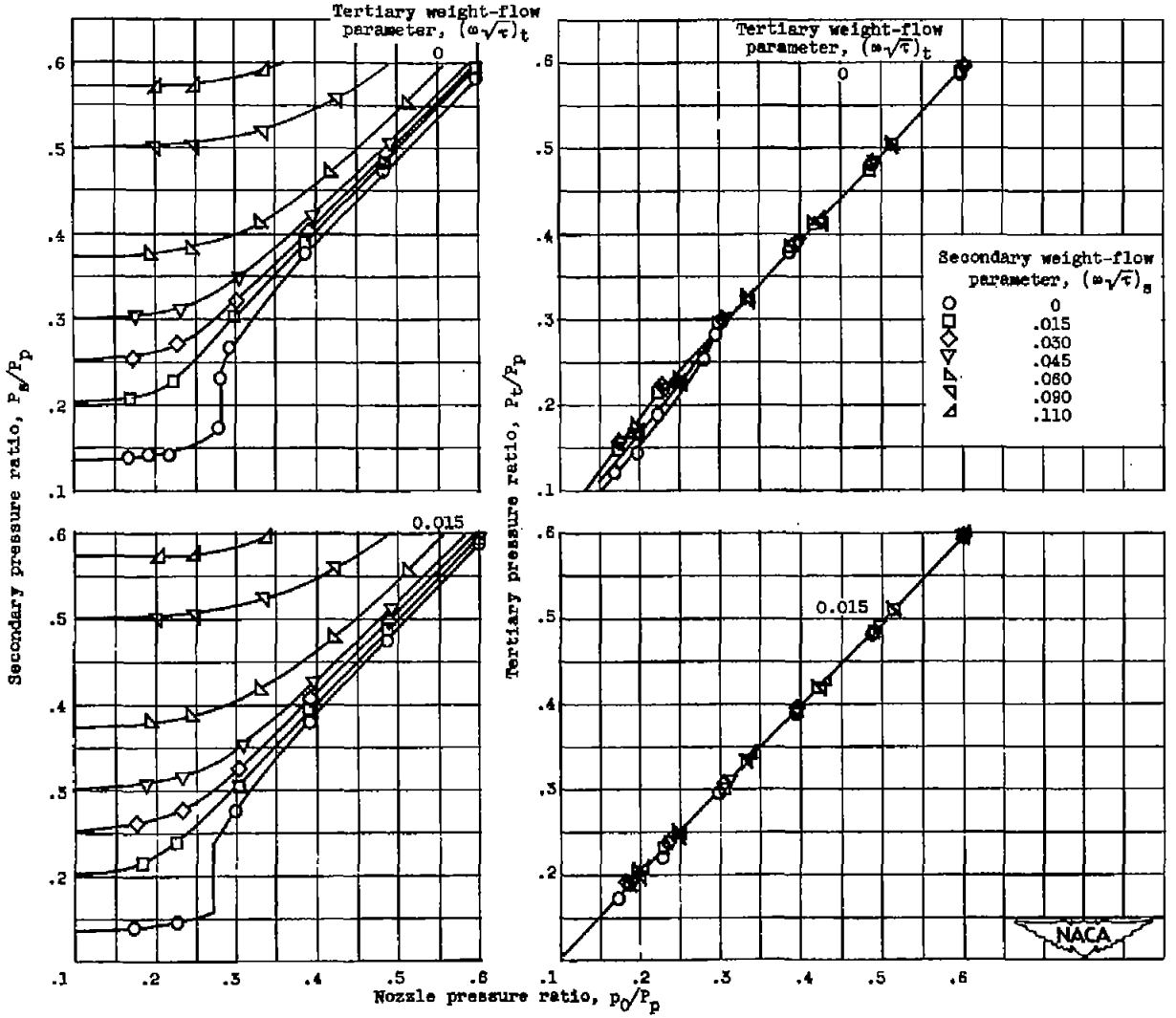

(d) Secondary-shroud-length ratio, 0.21; tertiary-shroud-length ratio, 0.54.

Figure 3. - Continued. Ejector performance curves.

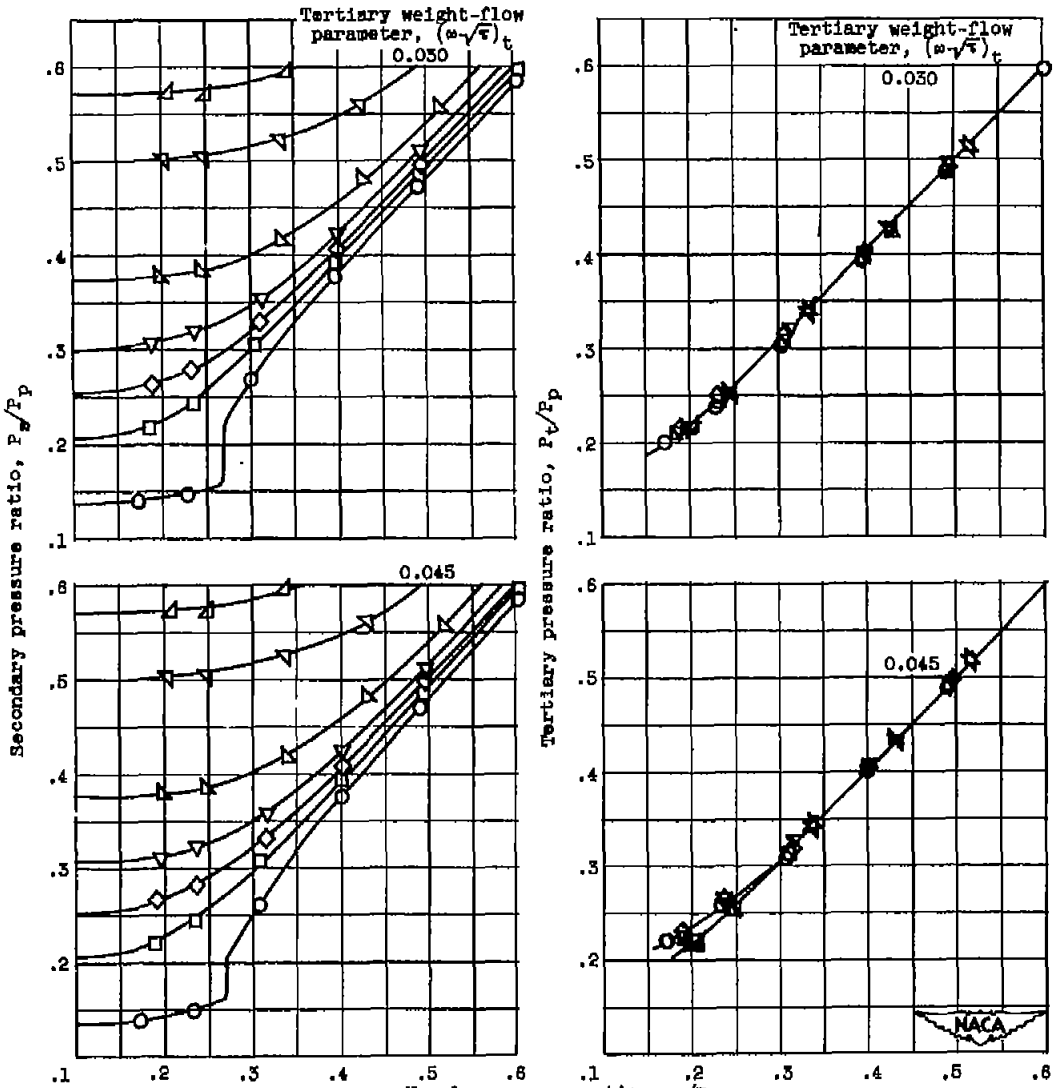

(d) Concluded. Secondary-shroud-length ratio, 0.21; tertiary-shroud-length ratio, 0.54.

Figure 3. - Continued. Ejector performance curves.

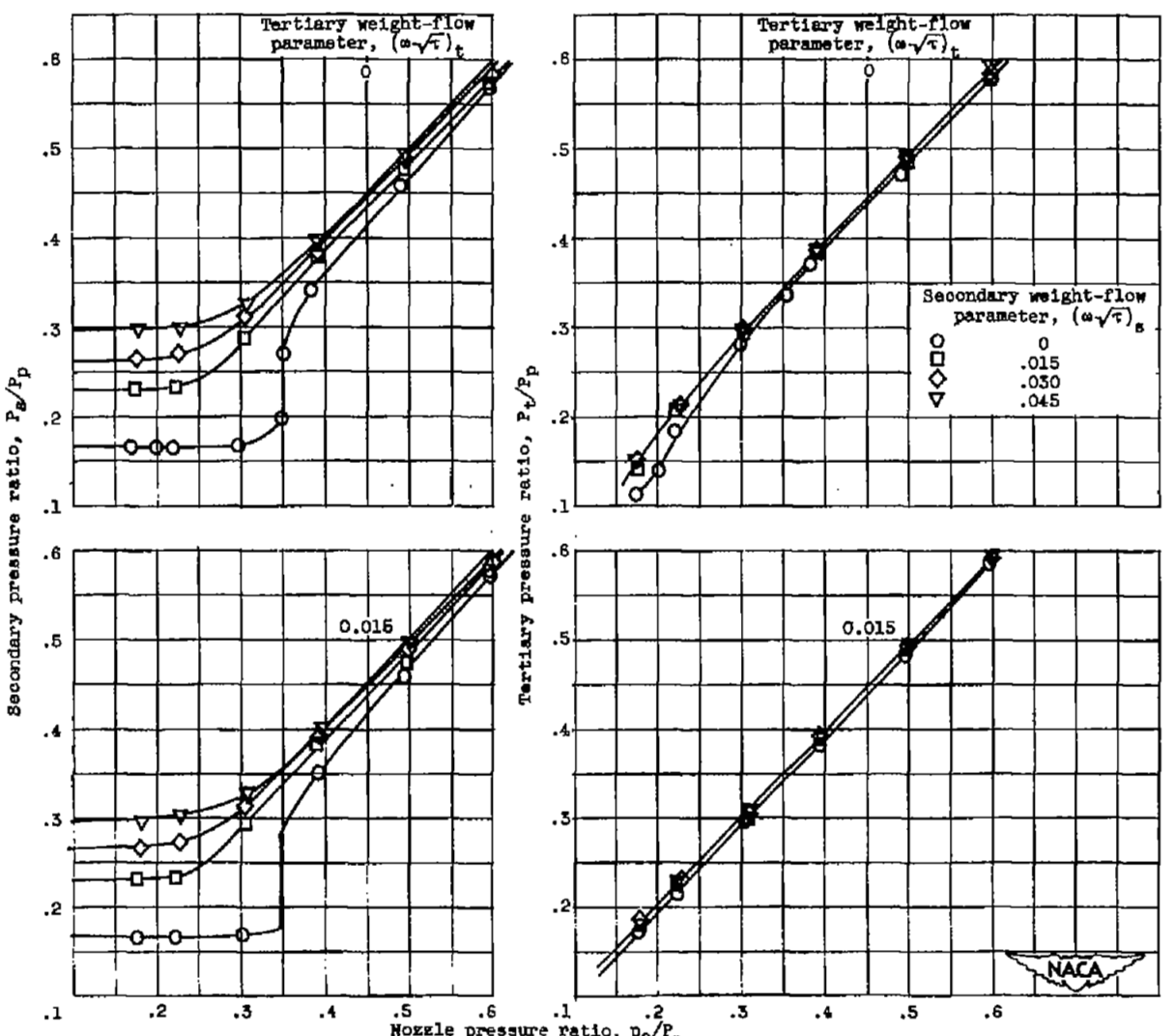

(e) Secondary-shroud-length ratio, 0.31; tertiary-shroud-length ratio, 0.84.

Figure 3. - Continued. Ejector performance curves.

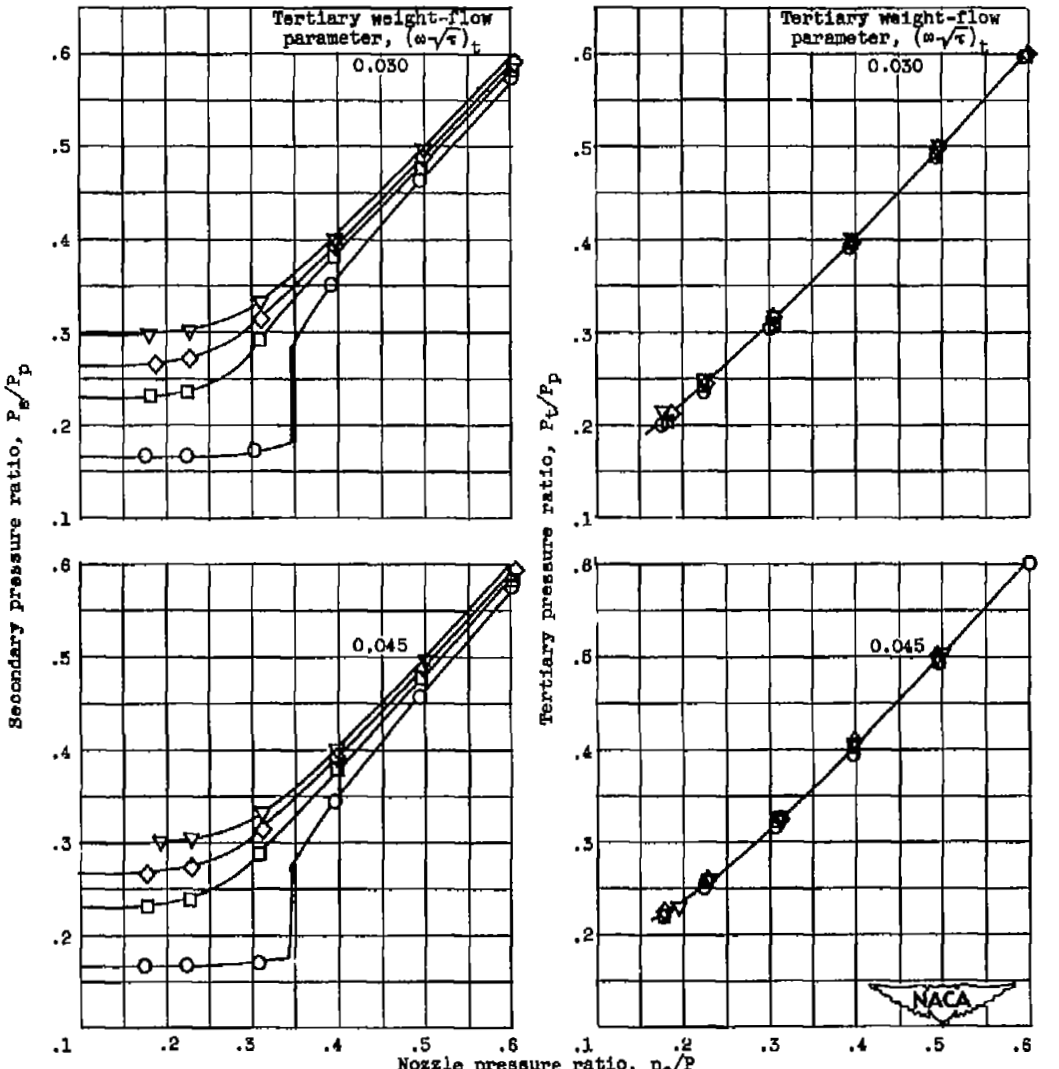

(e) Concluded. Secondary-shroud-length ratio, 0.31; tertiary-shroud-length ratio, 0.64.

Figure 3. - Continued. Ejector performance curves.

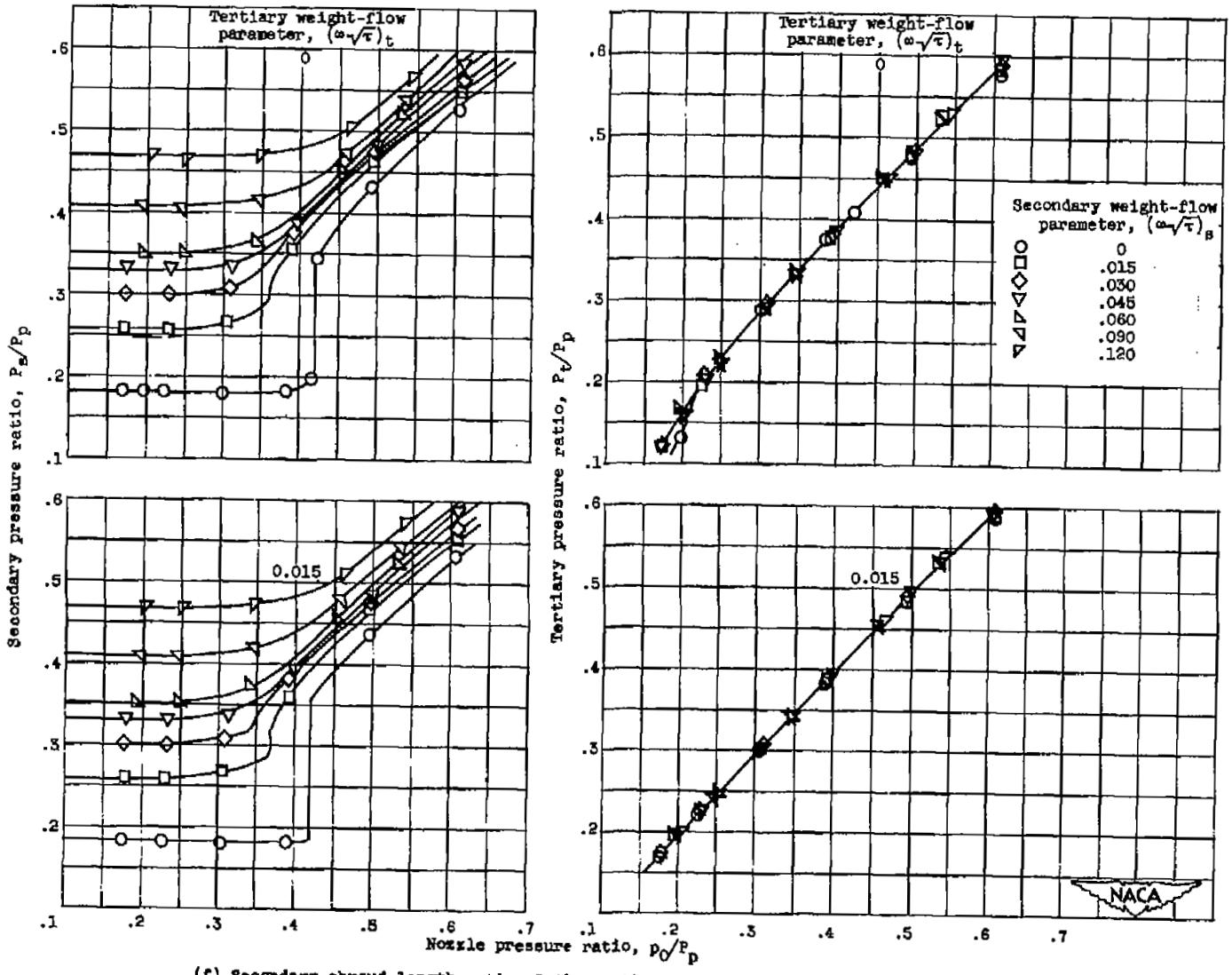

(f) Secondary-shroud-length ratio, 0.41; tertiary-shroud-length ratio, 0.74.

Figure 5. - Continued. Ejector performance curves.

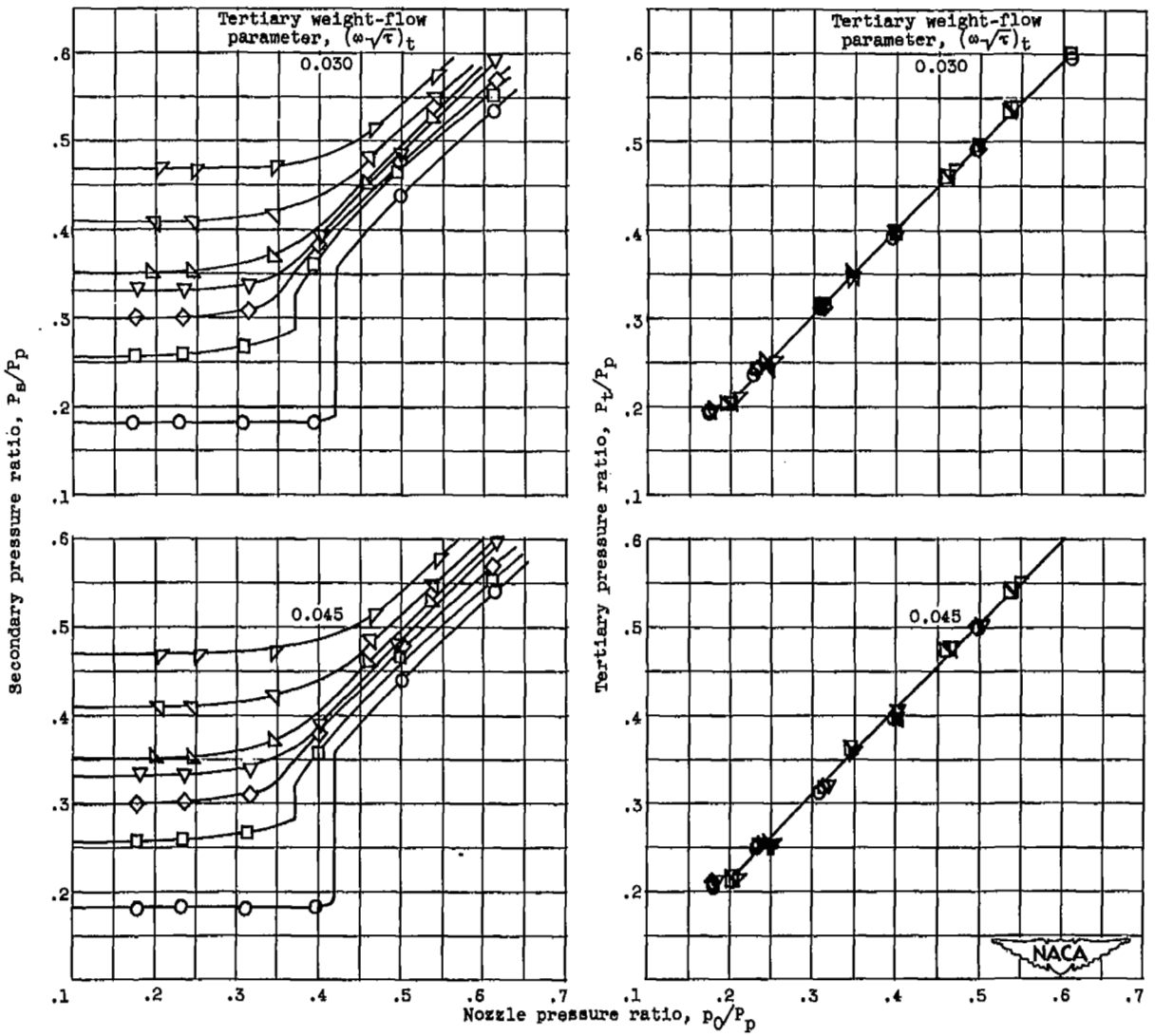

(f) Concluded. Secondary-shroud-length ratio, 0.41; tertiary-shroud-length ratio, 0.74.

Figure 3. - Continued. Ejector performance curves.

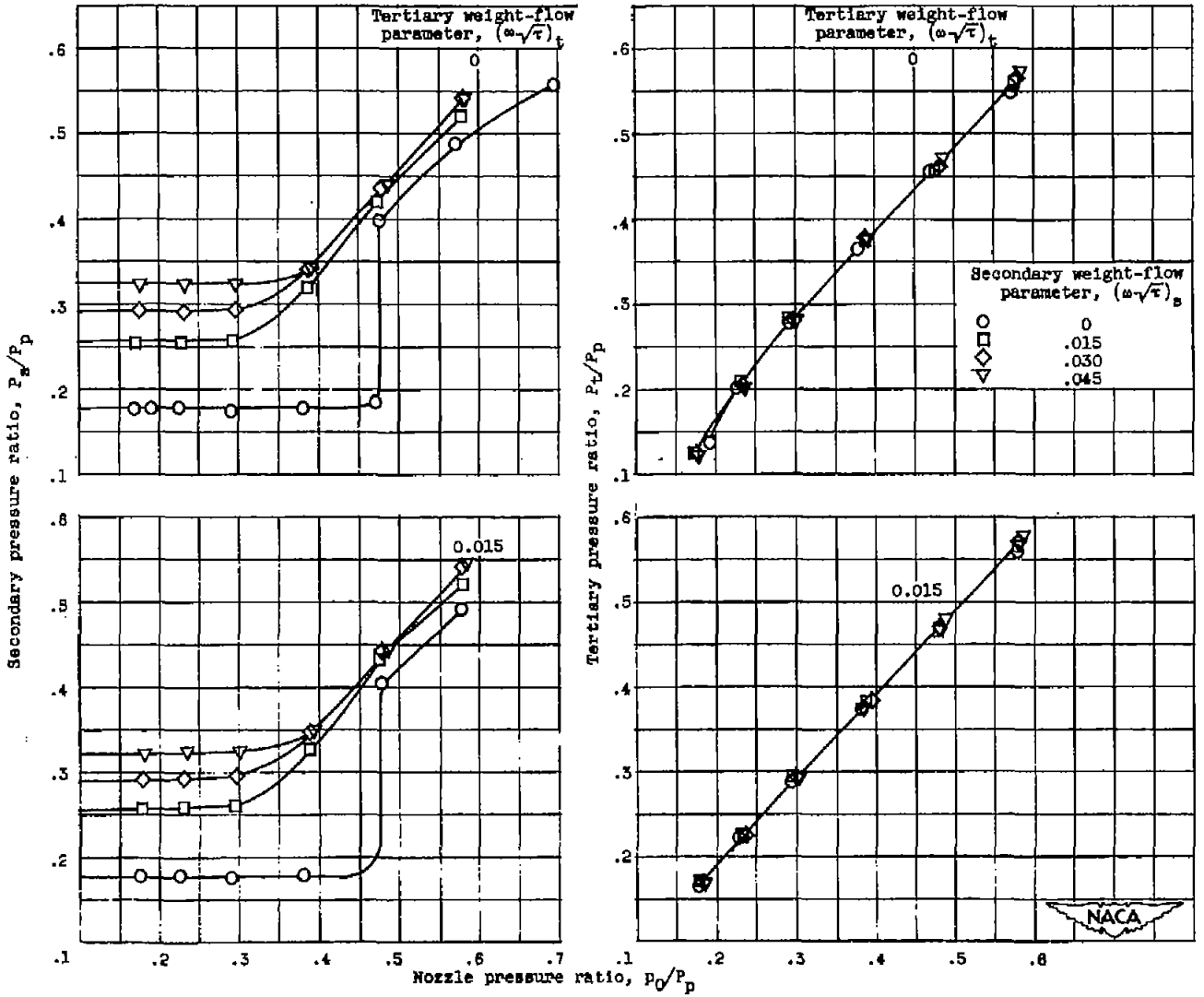

(g) Secondary-shroud-length ratio, 0.51; tertiary-shroud-length ratio, 0.84.

Figure 3. - Continued. Ejector performance curves.

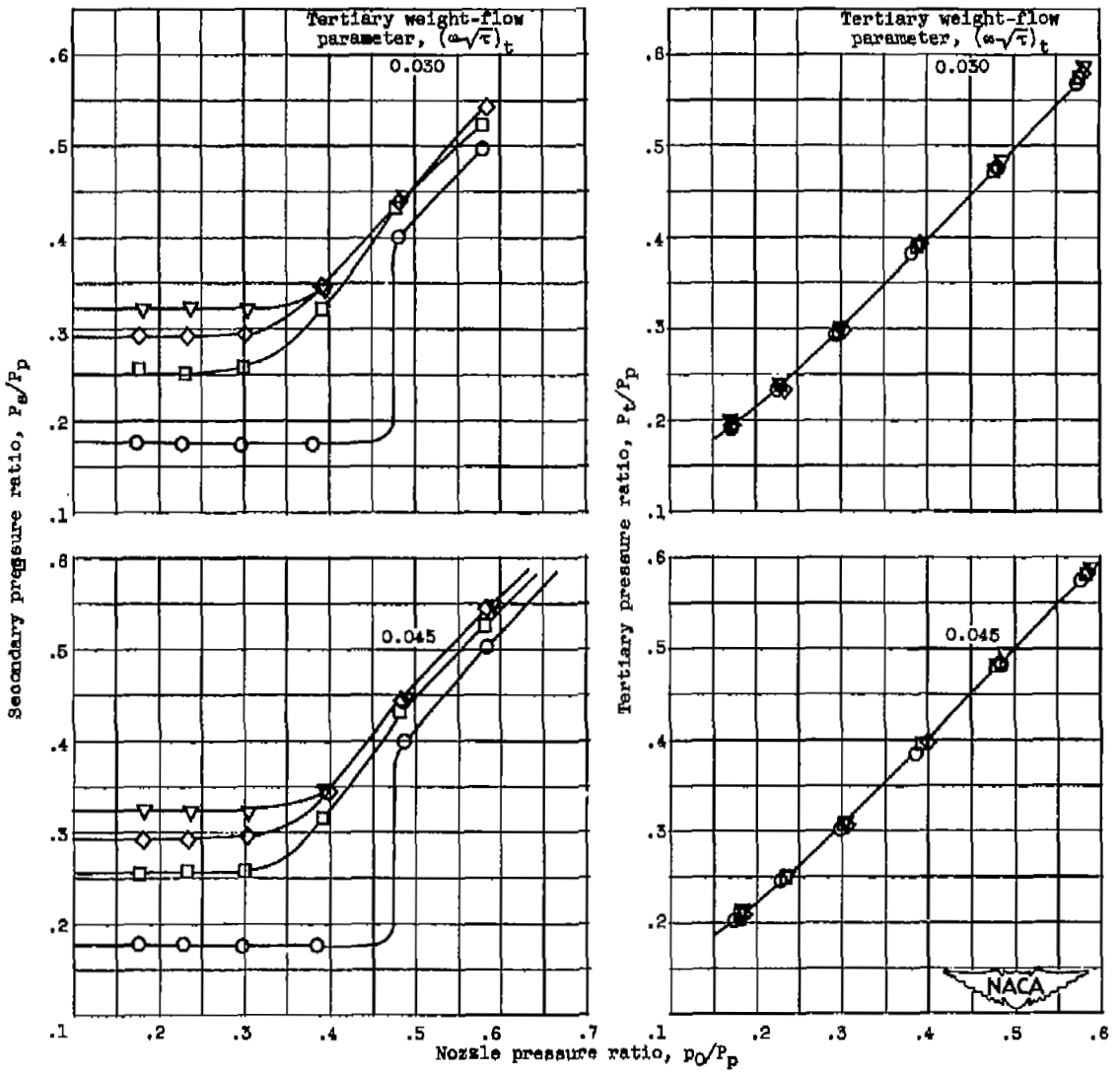

(g) Concluded. Secondary-shroud-length ratio, 0.51; tertiary-shroud-length ratio, 0.84.

Figure 3. - Continued. Ejector performance curves.

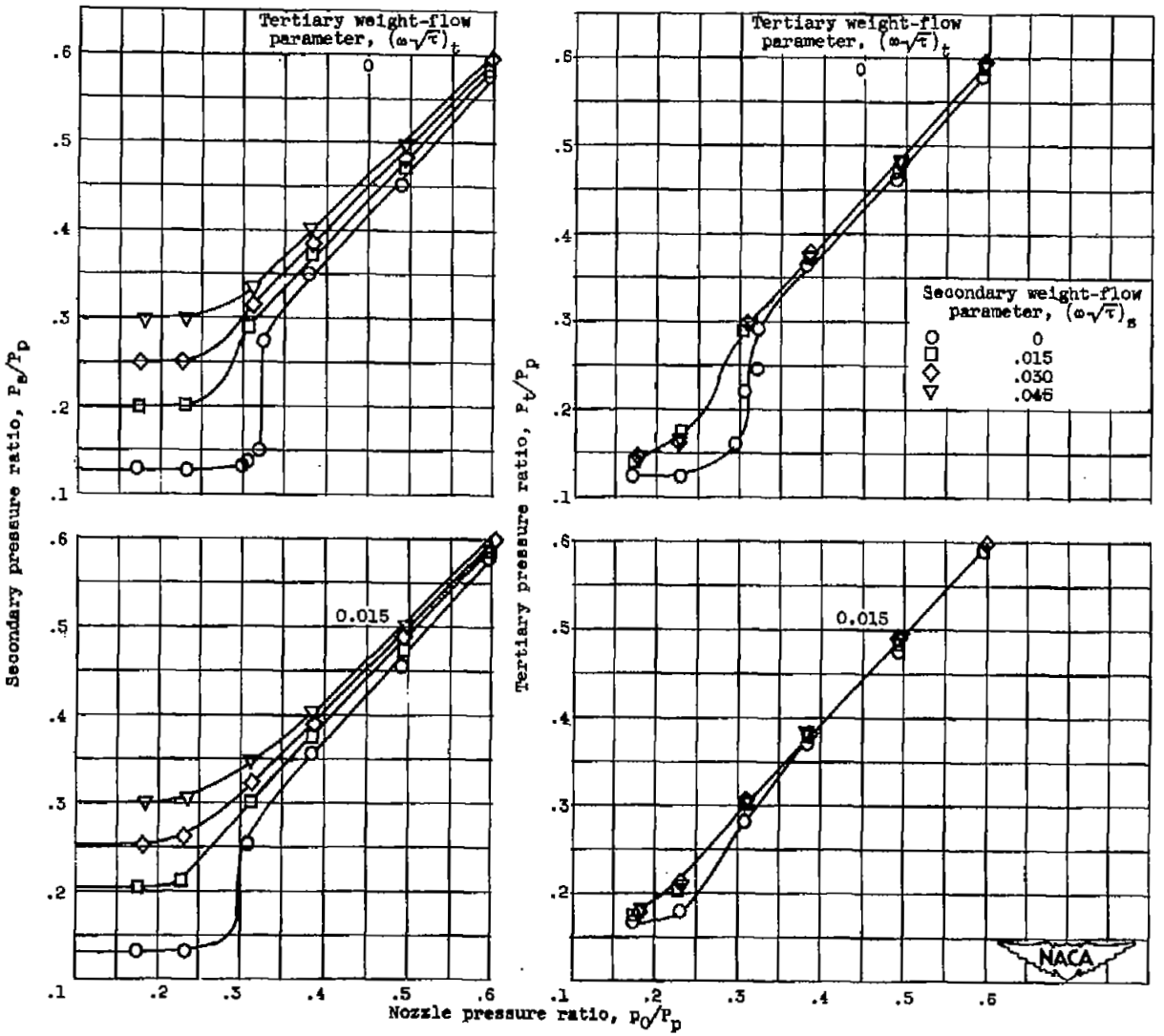

(h) Secondary-shroud-length ratio, 0.21; tertiary-shroud-length ratio, 0.72.

Figure 3. - Continued. Ejector performance curves.

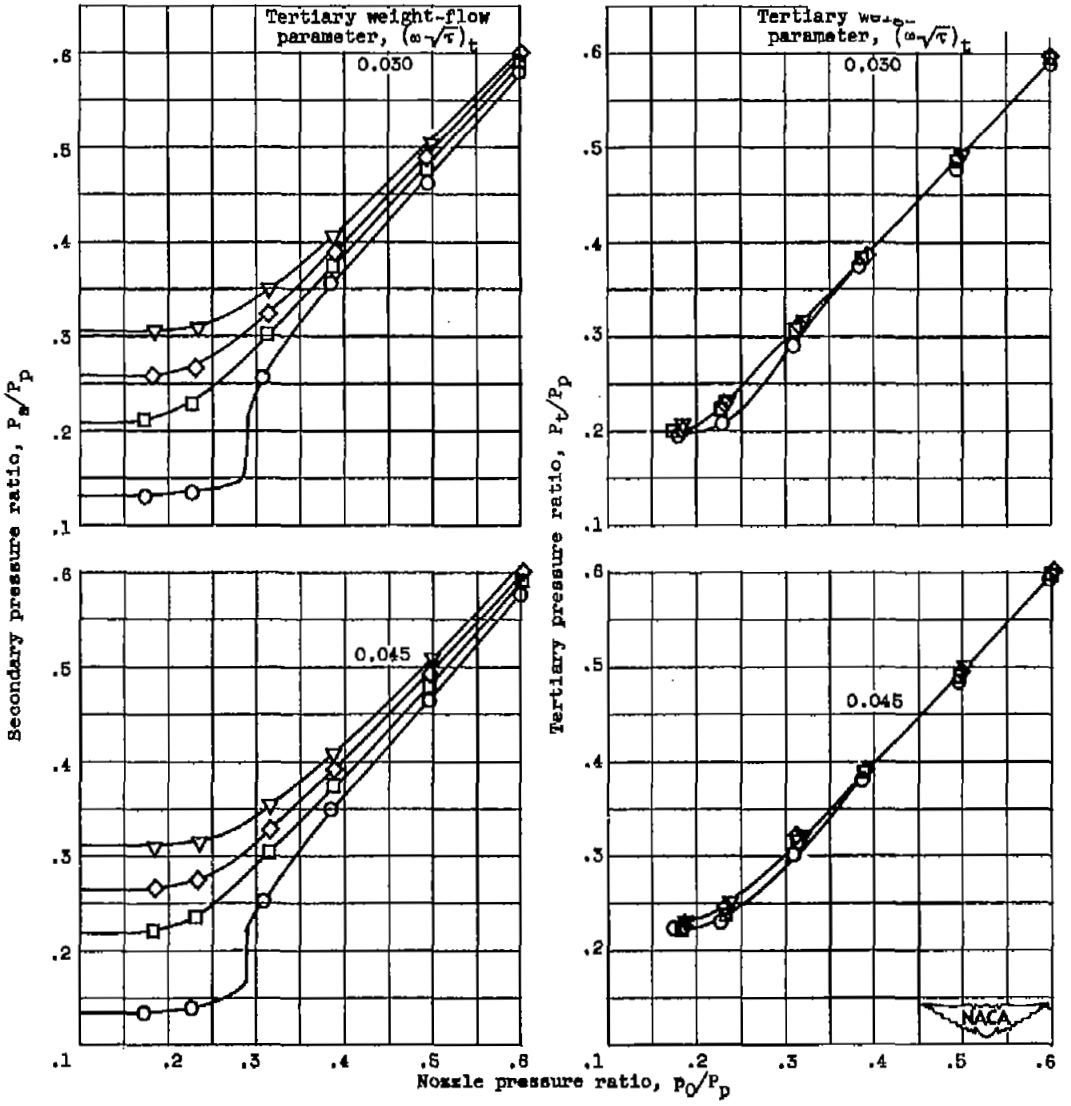

(h) Concluded. Secondary-shroud-length ratio, 0.21; tertiary-shroud-length ratio, 0.72.

Figure 3. - Continued. Ejector performance curves.

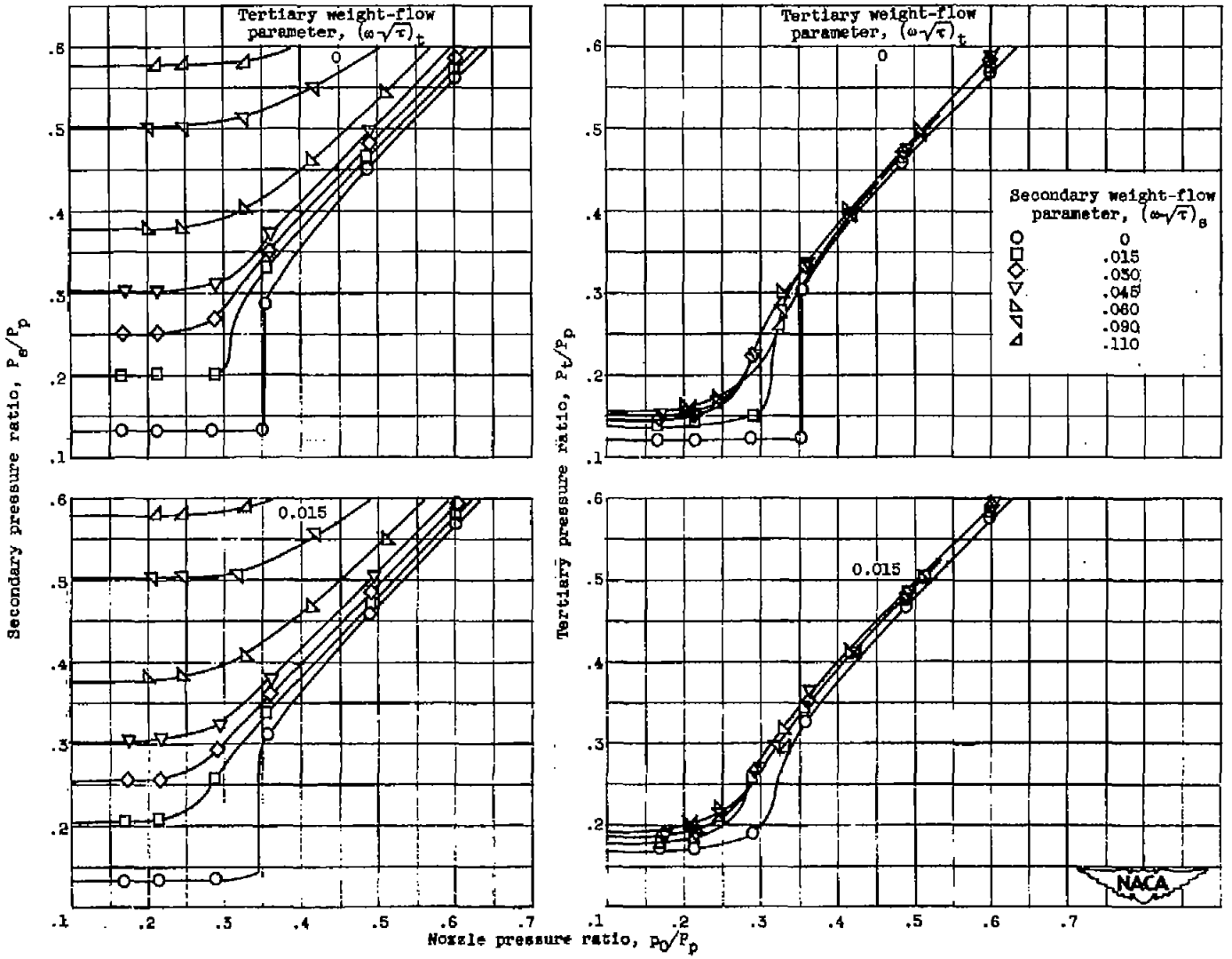

(i) Secondary-shroud-length ratio, 0.21; tertiary-shroud-length ratio, 0.90.

Figure 3. - Continued. Ejector performance curves.

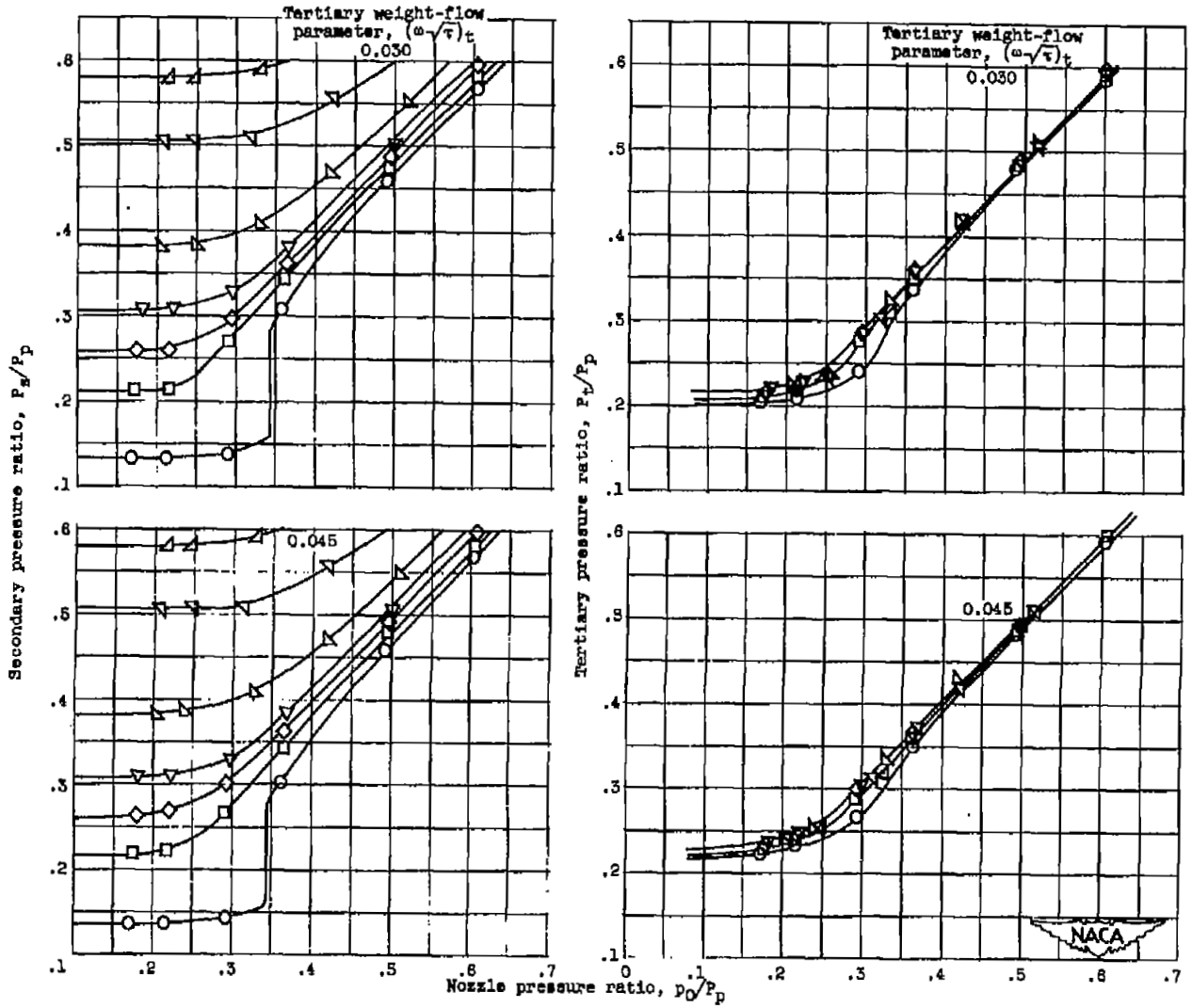

(i) Concluded. Secondary-shroud-length ratio, 0.21; tertiary-shroud-length ratio, 0.90.

Figure 3. - Continued. Ejector performance curves.

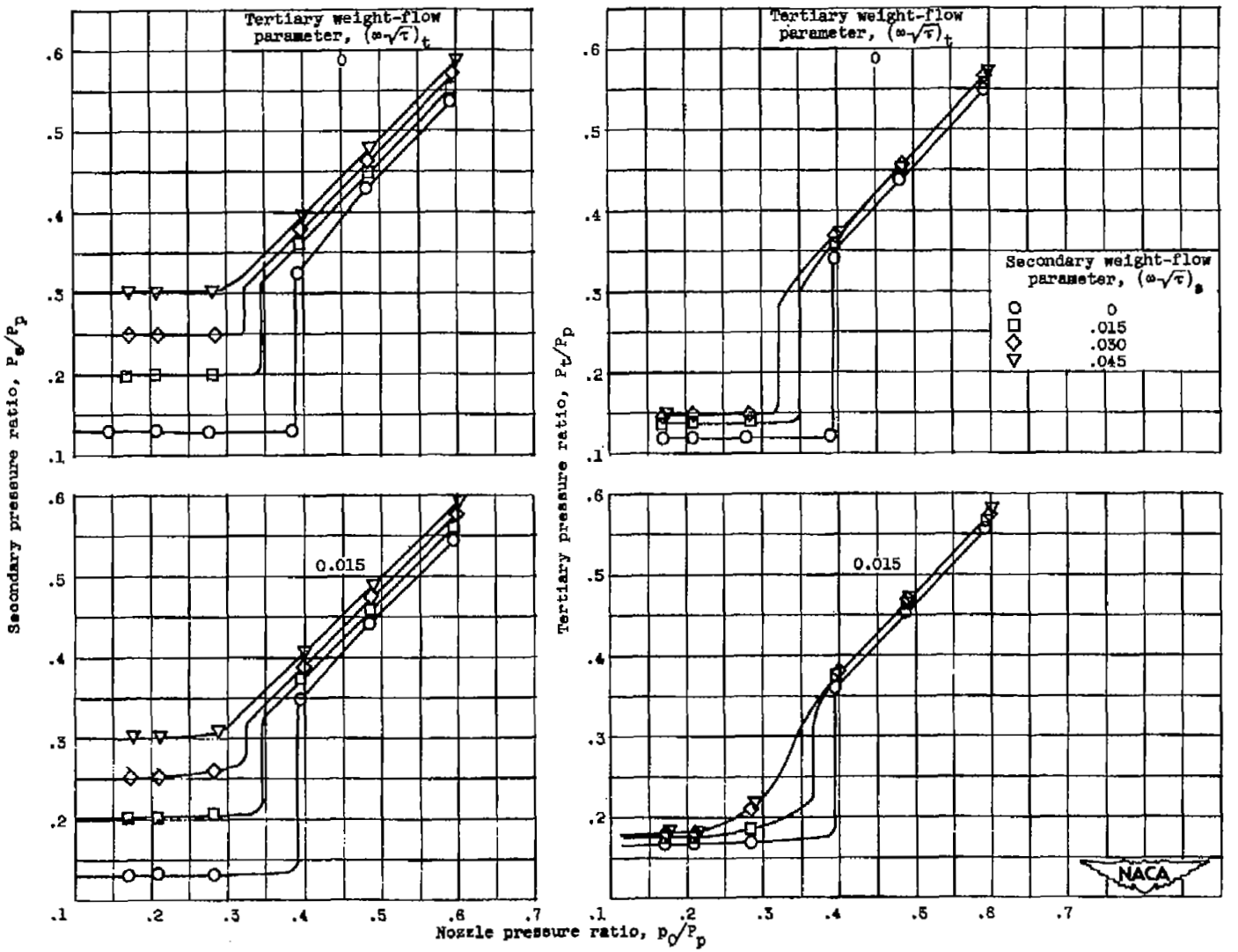

(j) Secondary-shroud-length ratio, 0.21; tertiary-shroud-length ratio, 1.07.

Figure 3. - Continued. Ejector performance curves.

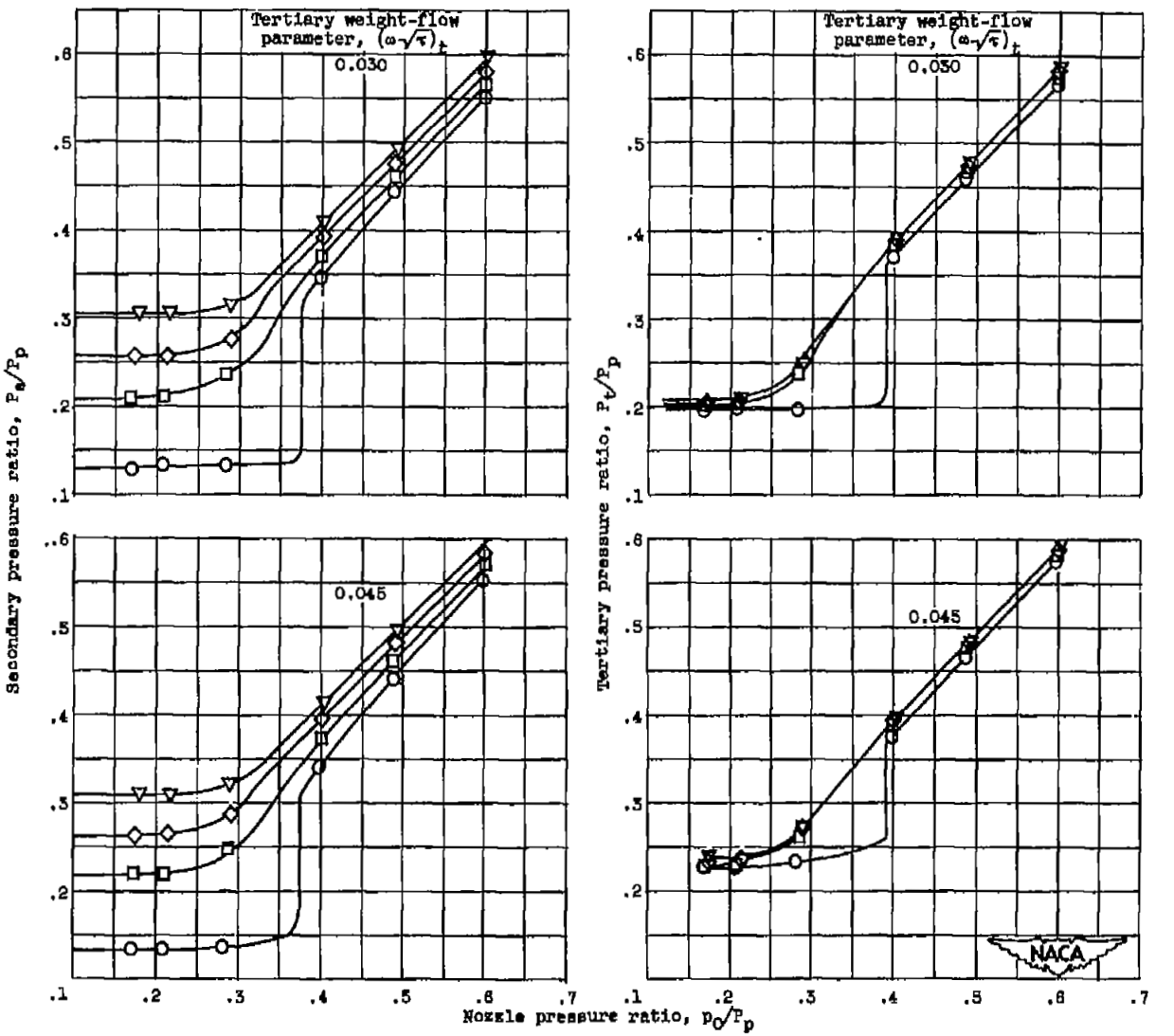

(j) Concluded. Secondary-shroud-length ratio, 0.21; tertiary-shroud-length ratio, 1.07.

Figure 3. - Concluded. Ejector performance curves.

3006

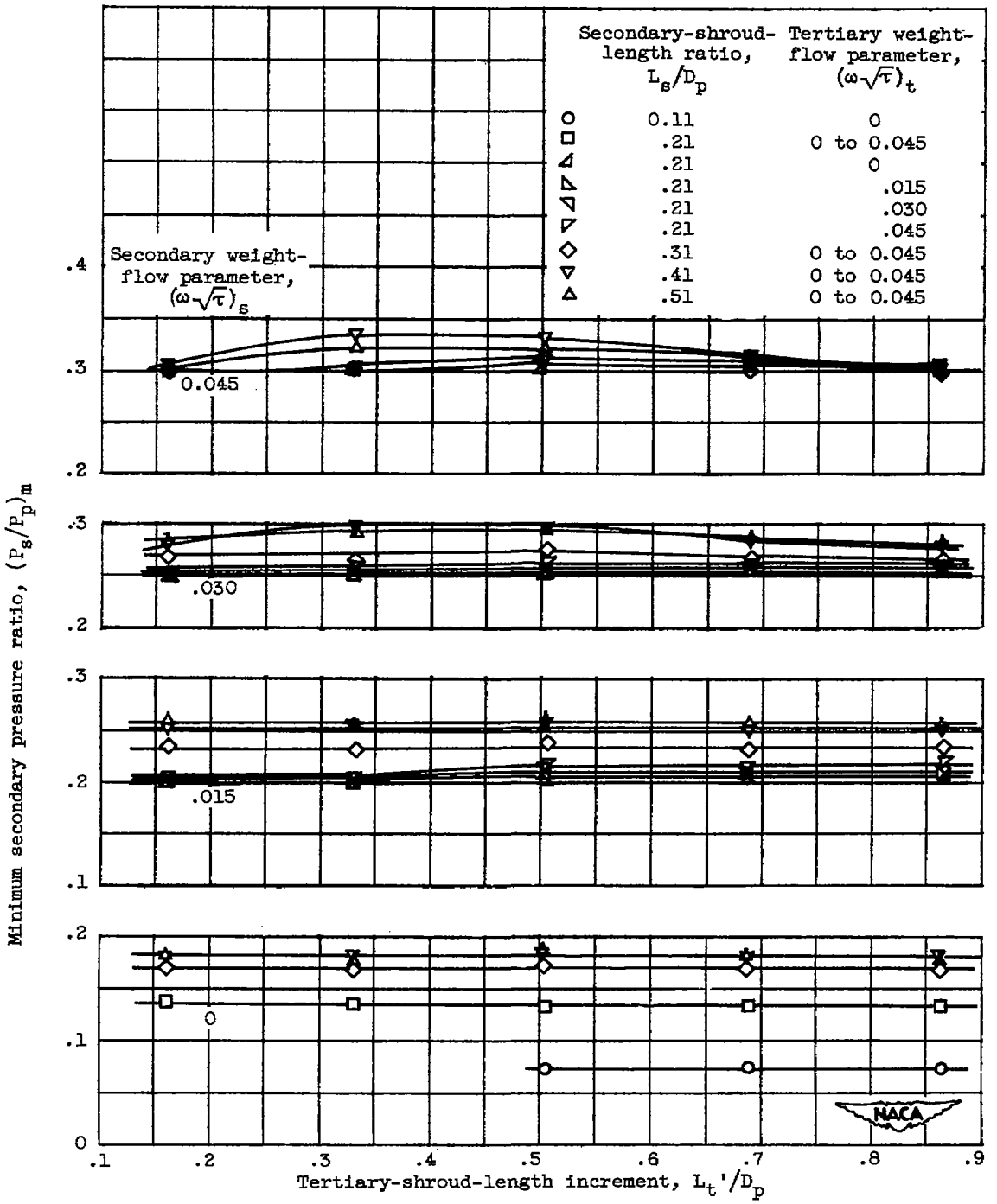

Figure 4. - Effect of tertiary-shroud length and weight flow on minimum secondary pressure ratio.

3006
CF-7 back

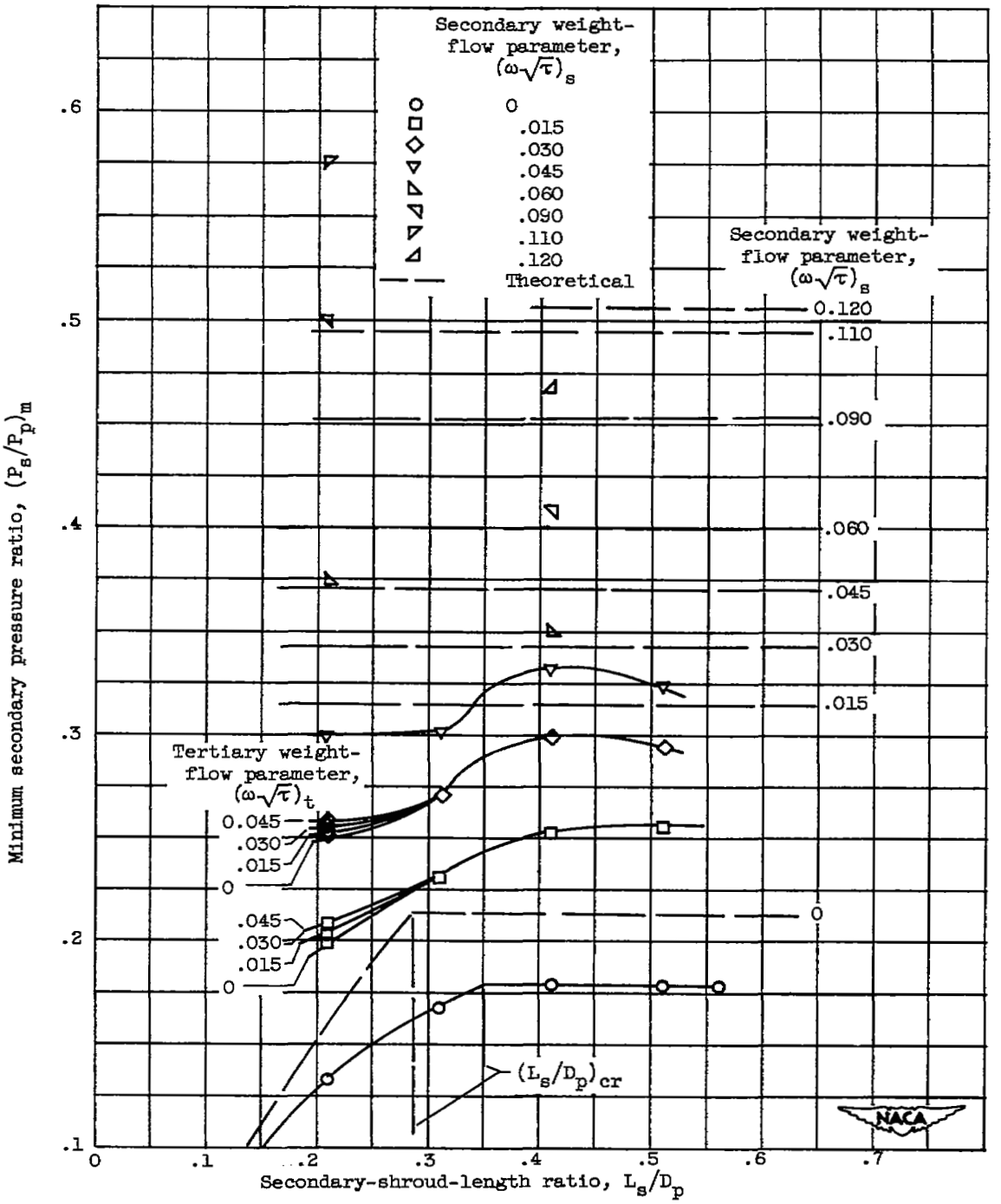

Figure 5. - Comparison of minimum secondary pressure ratios with values obtained from double-shroud ejector theory.

[redacted]

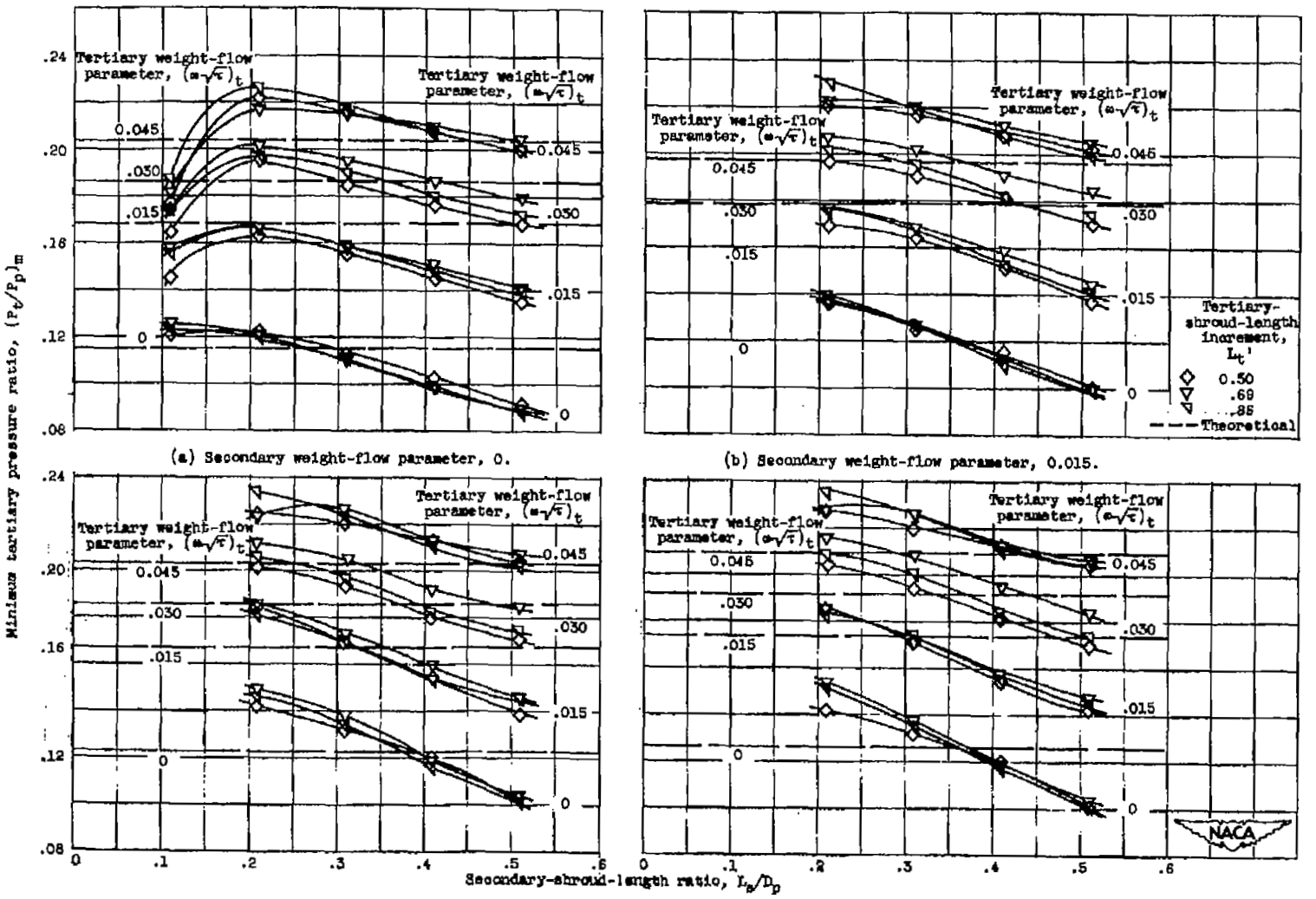

(a) Secondary weight-flow parameter, 0.

(b) Secondary weight-flow parameter, 0.015.

(c) Secondary weight-flow parameter, 0.030.

(d) Secondary weight-flow parameter, 0.045.

Figure 8. - Comparison of minimum tertiary pressure ratios with values obtained from double-shroud ejector theory.

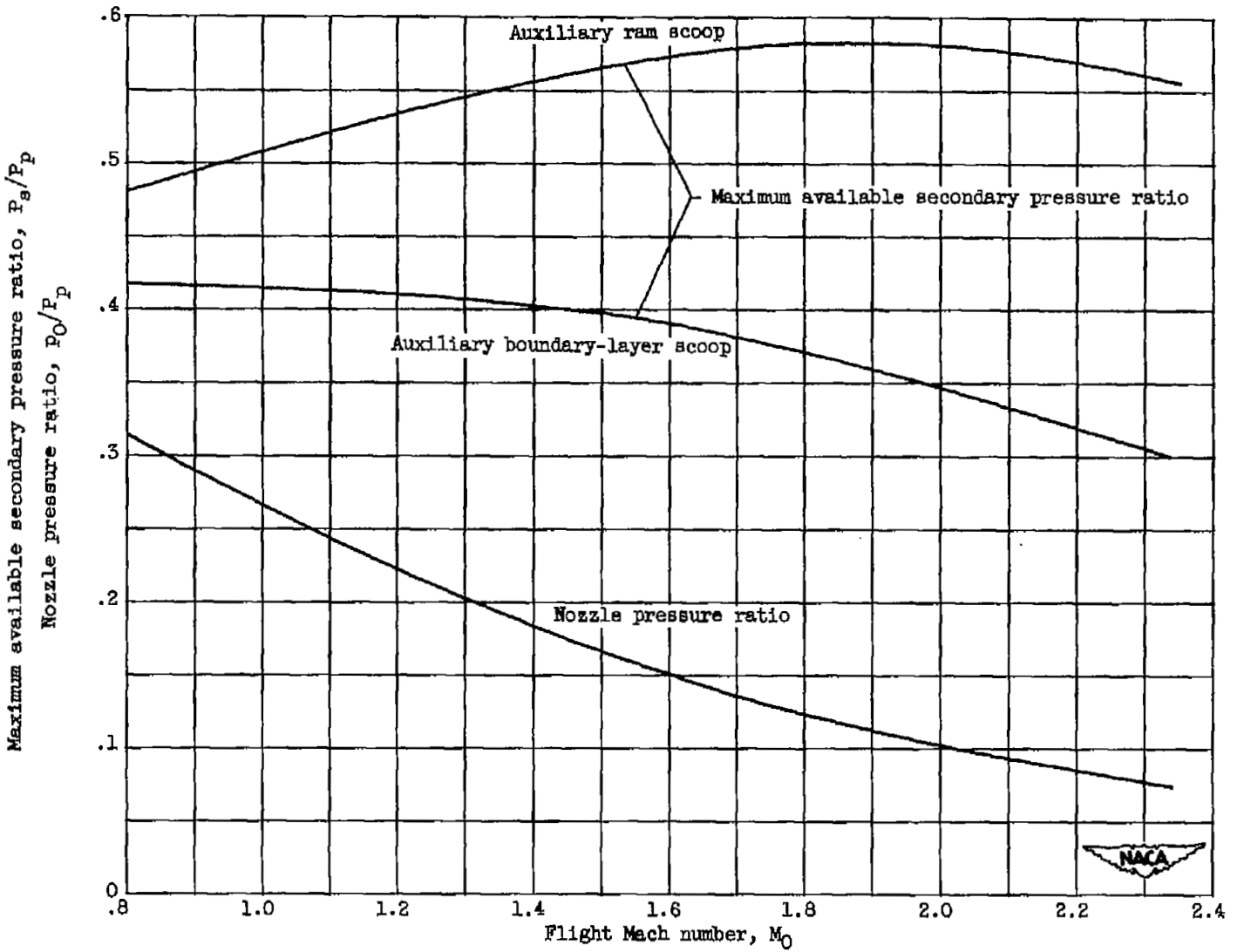

Figure 7. - Flight-plan assumptions.

3006

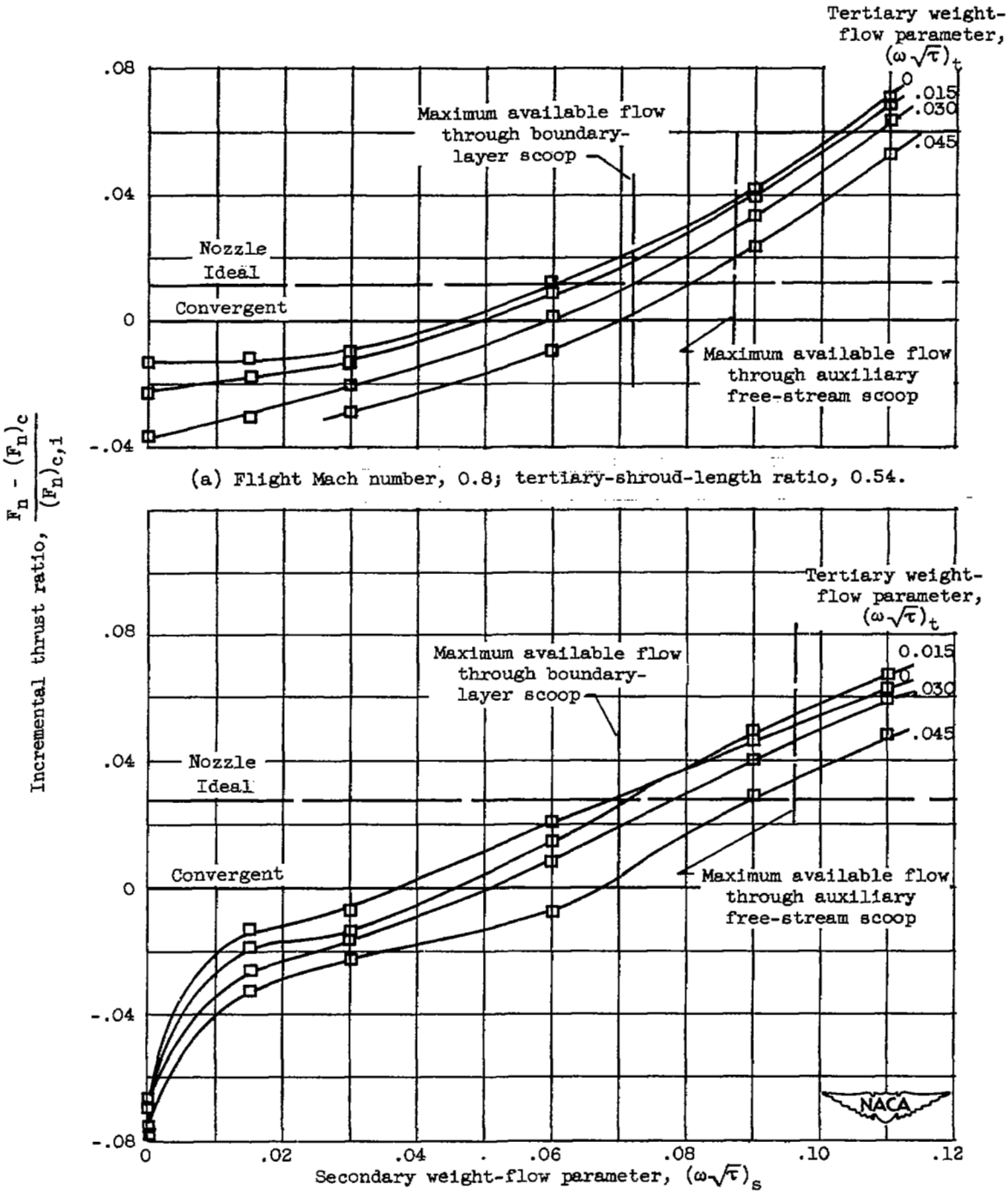

Figure 8. - Variation of incremental thrust ratio with ejector parameters at various flight Mach numbers. Secondary-shroud-length ratio, 0.21.

[redacted]

3006

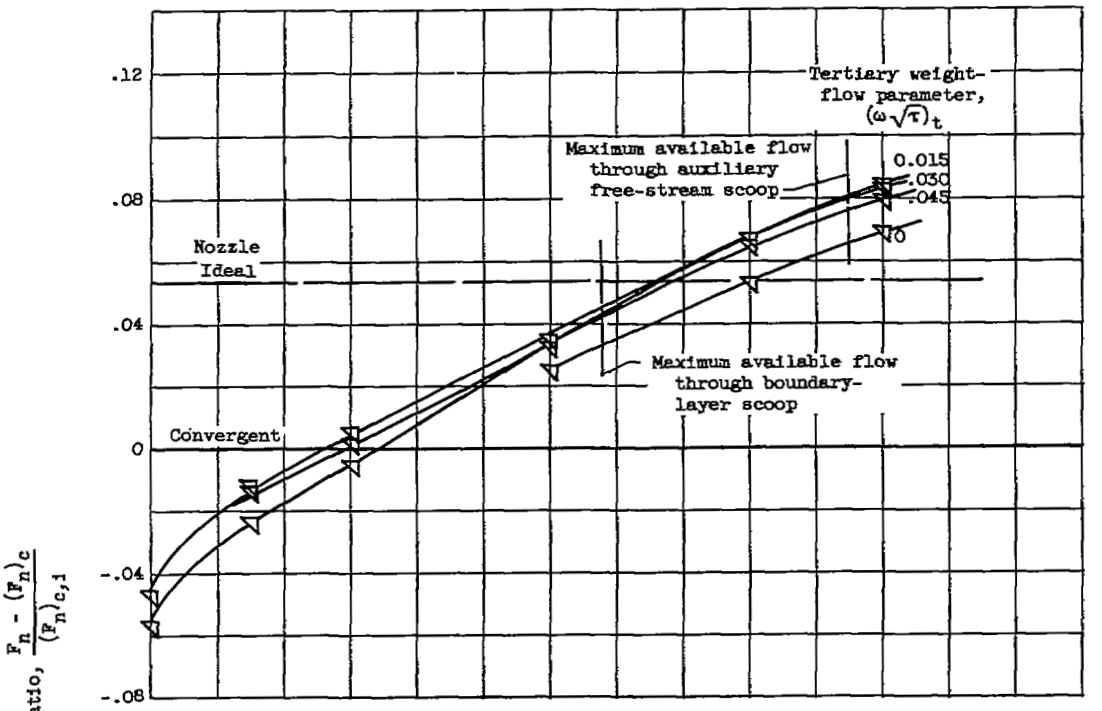

(c) Flight Mach number, 1.4; tertiary-shroud-length ratio, 0.90.

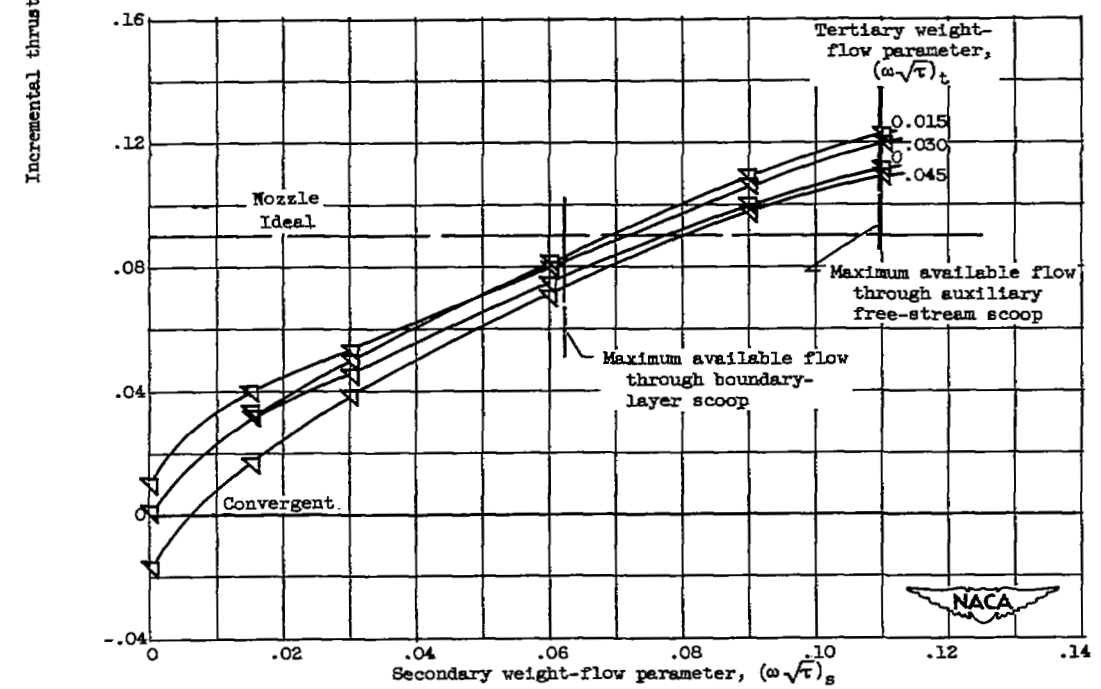

Incremental thrust ratio, $\frac{F_n - (F_n)_c}{(F_n)_{c,i}}$

(d) Flight Mach number, 1.7; tertiary-shroud-length ratio, 0.90.

Figure 8. - Continued. Variation of incremental thrust ratio with ejector parameters at various flight Mach numbers. Secondary-shroud-length ratio, 0.21.

[redacted]

3006

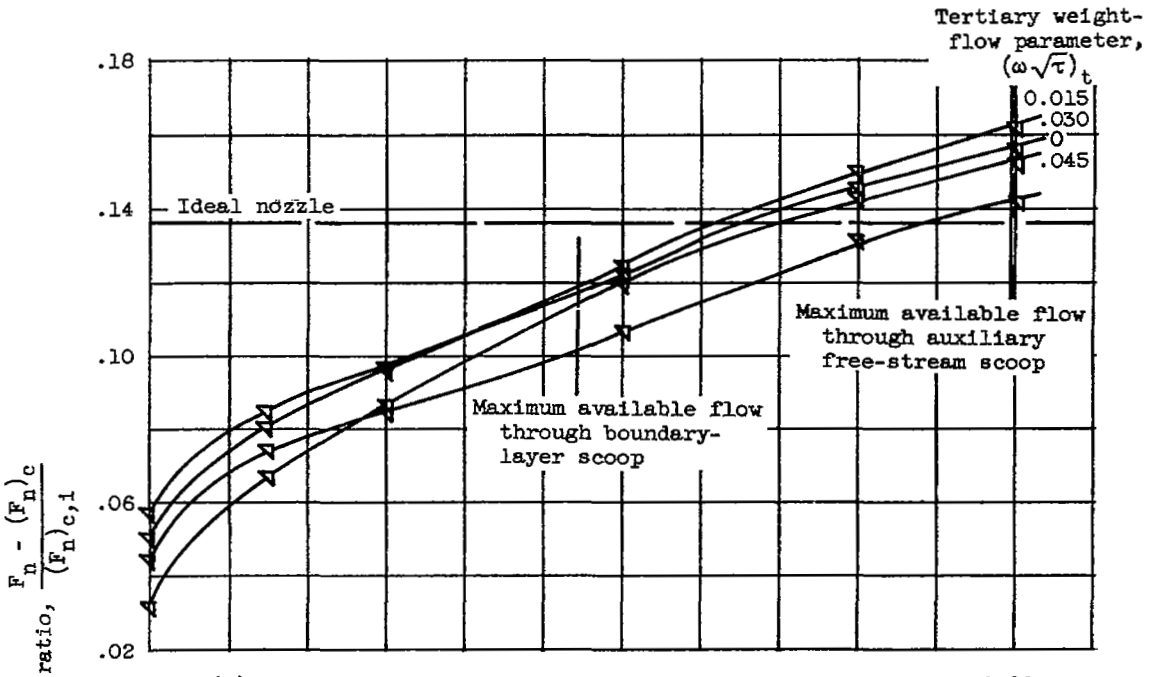

(e) Flight Mach number, 2.0; tertiary-shroud-length ratio, 0.90.

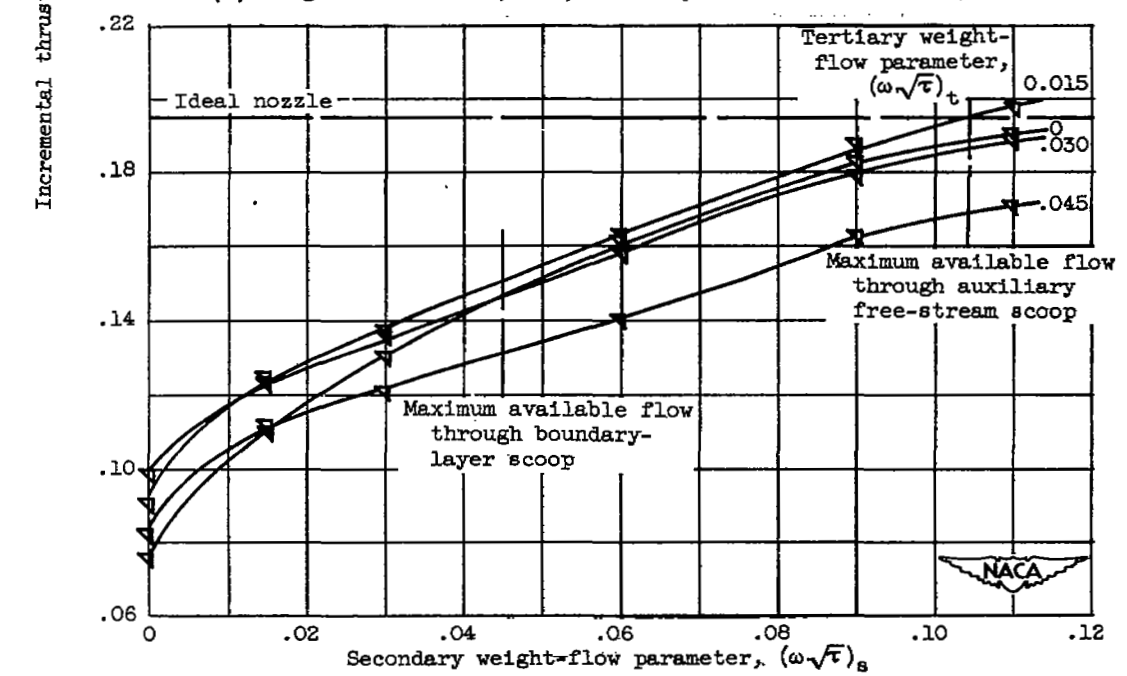

(f) Flight Mach number, 2.3; tertiary-shroud-length ratio, 0.90.

Figure 8. - Concluded. Variation of incremental thrust ratio with ejector parameters at various flight Mach numbers. Secondary-shroud-length ratio, 0.21.

NACA-Langley - 11-24-53 - 325

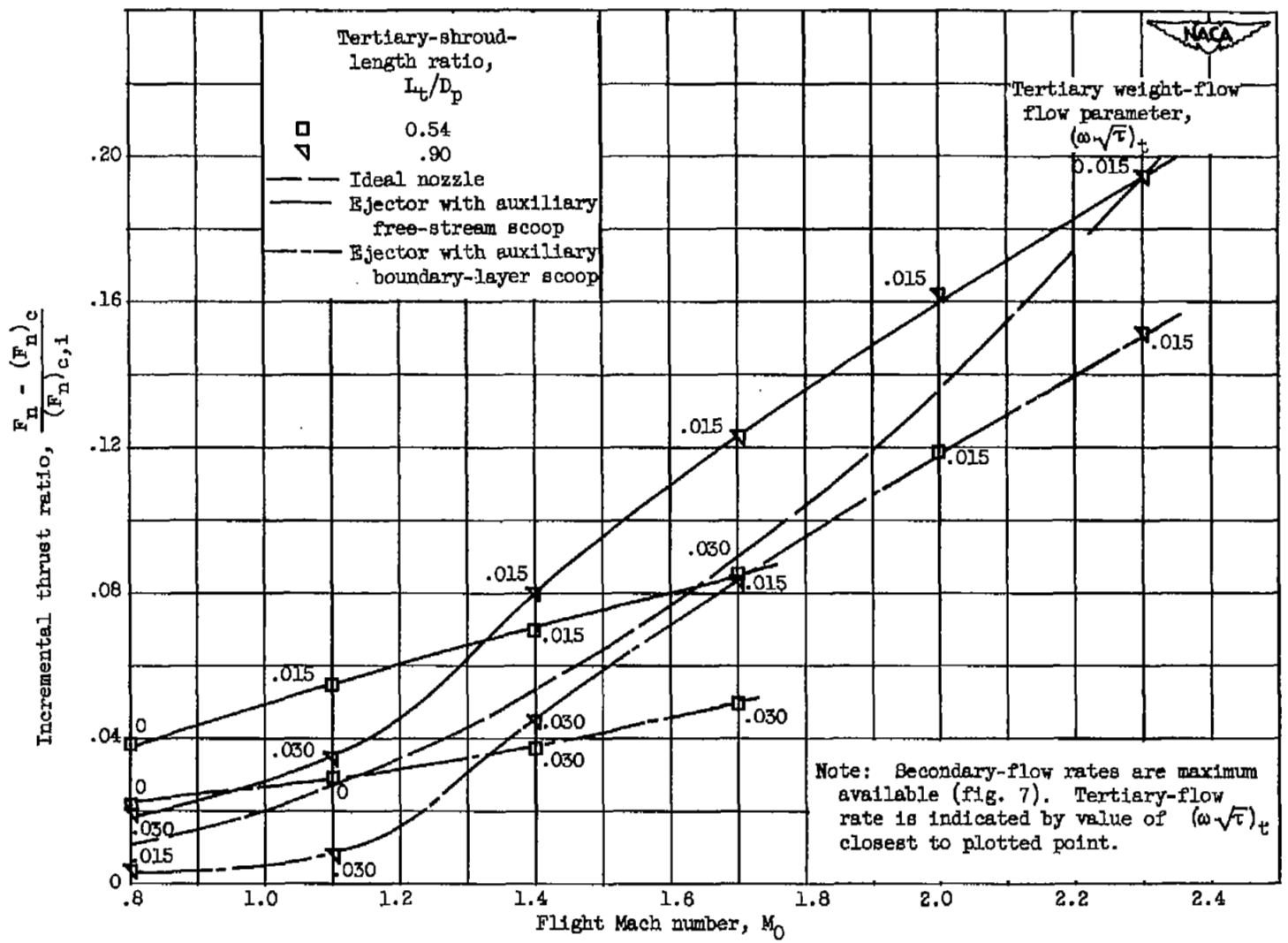

Figure 9. - Variation of incremental thrust ratio for various ejector configurations. Secondary-shroud-length ratio, 0.21.

SECURITY INFORMATION

NASA Technical Library
3 1176 01435 2836

[redacted]